Supporting Information

Persistent, Highly Localized, and Tunable [4]Helicene Radicals

Aslam C. Shaikh,[a] Jules Moutet,[a] José M. Veleta,[a] Md Mubarak Hossain,[a] Jan Bloch,[b] Andrei V. Astashkin,[a] and Thomas L. Gianetti*[a]

[a]Department of Chemistry and Biochemistry, University of Arizona, Tucson, AZ, United States.

[b]Department of Chemistry and Applied Biosciences, ETH Zürich, Zürich, Switzerland

*Email: tgianetti@arizona.edu

Table of Contents

I. General information

Unless otherwise stated, the syntheses of radicals were carried out in oven-dried vials or reaction vessels loaded with magnetic stirring bars inside an N_2 filled glove box. Dried solvents and liquid reagents were transferred by oven-dried or hypodermic syringes. Experiments were monitored by analytical thin layer chromatography (TLC), on pre-coated silica gel plates. After elution, plates were revealed under UV light with 254 nm wavelength. Melting points are uncorrected and recorded using digital Buchi Melting Point Apparatus B-540. ^{1}H and ^{13}C NMR spectra and were recorded on Bruker AVII 400/500, spectrometers in deuterated solvents using TMS as internal standard, or the solvent residue signals as secondary standards, and the chemical shifts are shown in δ scales. Multiplicities of the ^{1}H NMR signals are denoted by s (singlet), d (doublet), dd (doublet of doublet), dt (doublet of triplet), t (triplet), quin (quintet), m (multiplet), br.s (broad singlet)… etc. HRMS (ESI) were performed via LTQ Orbitrap Velos ETD mass-spectrometer (ThermoFisher Scientific, Bremen, Germany). Single-crystal X-ray diffraction data were collected on either a Bruker Kappa APEX II CCD diffractometer using Mo K_α radiation (λ = 0.71073Å) radiation, or a Bruker AXS single-crystal system equipped with a Excillum METALJET liquid gallium X-ray source, kappa goniometer, Oxford 800 series cryostream set to 100 K, and Photon III detector. Image collection, data reduction, and scaling were performed with Bruker AXS APEX3 software. Compounds were drawn using ChemDraw and the assignments of NMR spectra were done on MestReNova. All the chemicals and solvents were purchased from Sigma Aldrich, Fisher Scientific, or VWR and used without further purification. Organic solvents used were dried by using a solvent purification system. The electrolyte tetrabutylammonium hexafluorophosphate (TBAF-PF_6) was recrystallized from ethanol three times prior to use. Compound **1** was prepared according to Laursen report.[1]

II. General synthetic procedure

II.1 Typical procedures for synthesis of 2-H$^+$, 2-NO$_2^+$, 3$^+$ and 5$^+$

Note: Compound **4**$^+$ was prepared according to previous report.[1] All the NMR spectra are provided in our previous report.[1b]

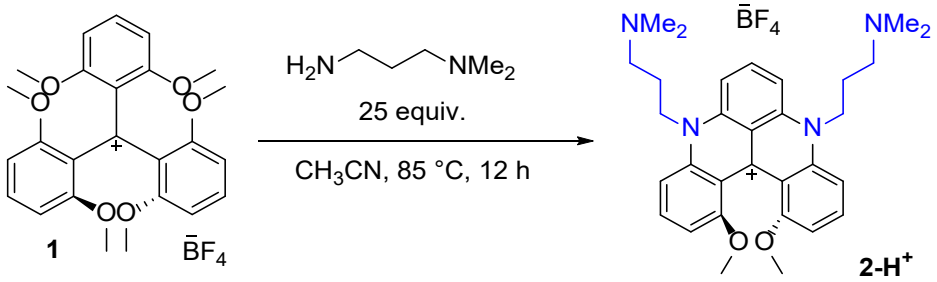

Racemic-5,9-bis(3-(dimethylamino)propyl)-1,13-dimethoxy-5,9-dihydro-13b*H*-quinolino[2,3,4-*kl*]acridin-13b-ylium tetrafluoroborate salt (2-H$^+$): *N,N*-dimethylpropane-1,3-diamine (6.28 ml, 49.46 mmol, 25 equiv) was added to a solution of tris(2,6 dimethoxyphenyl)carbenium tetrafluoroborate (1.00 g, 1.99 mmol, 1.0 equiv) in anhydrous acetonitrile (15 ml). The reaction mixture was heated at 85 °C for 12 hours then allowed to cool to room temperature. The crude product precipitated upon addition of Et_2O (~100 ml). The precipitate was filtered and washed several times with Et_2O, dried and collected. Selective precipitation by addition of Et_2O to a solution of crude product in CH_3CN afforded the dimethoxyquinacridinium tetrafluoroborate salts (1.12 g, 96%).

Grey solid; Melting point: 218-220 °C; R_f= 0.12 (SiO_2, CH_2Cl_2:MeOH (80:20));

^{1}H NMR (400 MHz, Acetonitrile-d_3) δ = 8.12 (t, *J* = 8.5 Hz, 1H), 7.88 (dd, *J* = 8.9, 8.0 Hz, 2H), 7.56 (dd, *J* = 15.9, 8.7 Hz, 4H), 6.90 (d, *J* = 8.0 Hz, 2H), 4.71 (ddd, *J* = 15.6, 9.9, 5.9 Hz, 2H), 4.50 (ddd, *J* = 15.5, 9.7, 5.9 Hz, 2H), 3.72 (s, 6H), 2.50 (t, *J* = 6.4 Hz, 4H), 2.28 (s, 12H), 2.12 (m, 4H).

^{13}C NMR (125 MHz, Acetonitrile-d_3) δ = 160.58, 143.43, 143.10, 139.90, 137.92, 137.33, 120.25, 113.86, 108.49, 105.86, 103.90, 57.16, 56.46, 48.99, 45.90, 25.14.

^{19}F NMR (376 MHz, Acetonitrile-d_3) δ = -152.71, -152.66.

HRMS(ESI): *m/z* = Calcd for $C_{31}H_{39}N_4O_2^+$ $[M]^+$ 499.3068, found 499.3056.

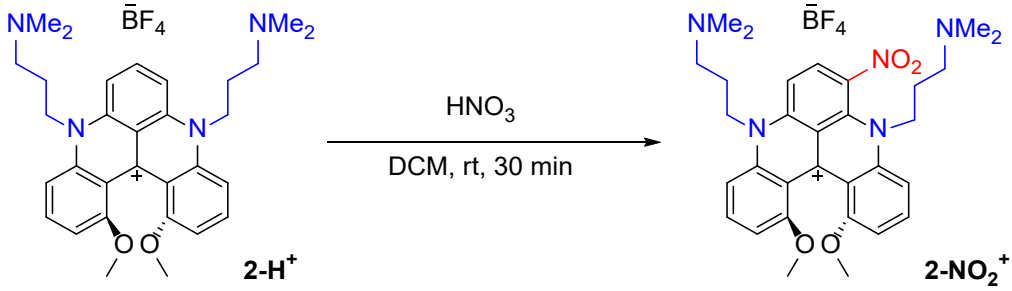

Racemic-5,9-bis(3-(dimethylamino)propyl)-1,13-dimethoxy-6-nitro-5,9-dihydro-13bH-quinolino[2,3,4-kl]acridin-13b-ylium tetrafluoroborate salt ($2\text{-}NO_2^+$): To a solution of **$2\text{-}H^+$** (500 mg) in CH_2Cl_2 (10 mL) was added aqueous HNO_3 (67%, 3 mL). After 30 min of stirring at 25 °C, the reaction mixture was quenched by addition of aqueous NaOH (1.0 M, 40 mL) and then extracted with CH_2Cl_2 (3 x 10 mL). Aqueous HBF_4 (1.0 M, 10 mL) was added to the combined organic layers, washed with NaOH (1.0 M, 20 mL) again, dried over Na_2SO_4, and evaporated under vacuum. The solid was precipitated using CH_2Cl_2 and Et_2O solvent mixture. After filtration a dark red solid was obtained (490 mg, 90 %). Layering with CH_2Cl_2 and *n*-hexanes yielded dark red crystals.

Melting point: 170-172 °C; R_f= 0.12 (SiO_2, CH_2Cl_2:MeOH (80:20));

^{1}H NMR (400 MHz, Methylene Chloride-d_2) δ = 8.79 (d, *J* = 9.6 Hz, 1H), 8.12 (t, *J* = 8.5 Hz, 1H), 7.99 (t, *J* = 8.4 Hz, 1H), 7.91 (d, *J* = 9.6 Hz, 1H), 7.81 (d, *J* = 8.9 Hz, 1H), 7.52 (d, *J* = 8.7 Hz, 1H), 7.10 (d, *J* = 8.1 Hz, 1H), 7.01 (d, *J* = 8.2 Hz, 1H), 4.99 (m, 2H), 4.88 (m, 1H), 3.84 (s, 3H), 3.79 (s, 3H), 3.73 (m, 1H), 2.54 (t, *J* = 5.9 Hz, 2H), 2.32 (s, 6H), 2.26 (br.s, 2H), 1.95 (m, 1H), 1.81 (m, 1H), 1.69 (m, 2H), 1.52 (s, 6H).

^{13}C NMR (100 MHz, Methylene Chloride-d_2) δ = 159.88, 159.58, 141.75, 141.73, 141.27, 141.21, 139.22, 137.75, 136.55, 134.17, 132.03, 120.49, 116.57, 113.95, 109.90, 108.42, 106.69, 105.42, 104.99, 56.35, 56.32, 56.29, 55.35, 54.38, 54.11, 53.84, 53.57, 53.30, 45.73, 44.97, 26.32, 25.88.

^{19}F NMR (376 MHz, Methylene Chloride-d_2) δ = -152.48, -152.53.

HRMS(ESI): *m/z*=Calcd for $C_{31}H_{38}N_5O_4^+$ $[M]^+$ 544.2918, found 544.2911.

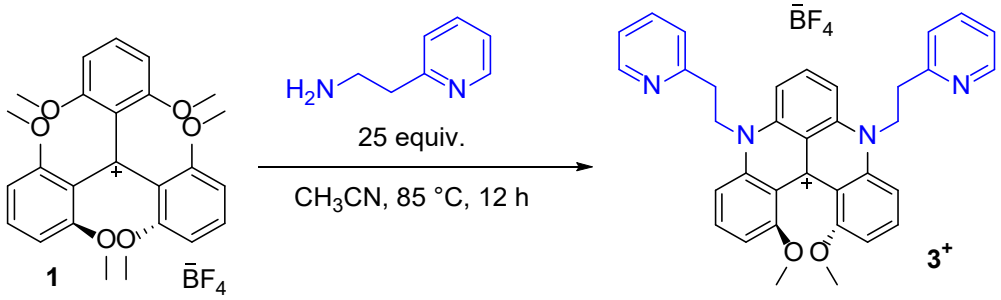

Racemic-1,13-dimethoxy-5,9-bis(2-(pyridin-2-yl)ethyl)-5,9-dihydro-13b*H*-quinolino [2,3,4-*kl*]acridin-13b-ylium tetrafluoroborate salt (3^+): *2-(pyridin-2-yl)ethan-1-amine* (5.97 ml, 49.75 mmol, 25 equiv) was added to a solution of tris(2,6 dimethoxyphenyl)carbenium tetrafluoroborate (1.00 g, 1.99 mmol, 1.0 equiv) in anhydrous acetonitrile (15 ml). The reaction mixture was heated at 85 °C for 12 hours then allowed to cool to room temperature. The crude product precipitated upon addition of Et_2O (~100 ml). The precipitate was filtered and washed several times with Et_2O, dried and collected. Selective precipitation by addition of Et_2O to a solution of the crude product in CH_2Cl_2 afforded the dimethoxyquinacridinium tetrafluoroborate salts (1.15 g, 92%).

Grey solid; Melting point: 228-230 °C; R_f = 0.5 (SiO_2, CH_2Cl_2:MeOH (90:10));

^{1}H NMR (400 MHz, Acetonitrile-d_3) δ = 8.56 (s, 2H), 8.21 (t, *J* = 8.5 Hz, 1H), 7.90 (t, *J* = 8.5 Hz, 2H), 7.77 (d, *J* = 8.5 Hz, 2H), 7.73 – 7.57 (m, 4H), 7.34 (d, *J* = 7.7 Hz, 2H), 7.24 (t, *J* = 6.4 Hz, 2H), 6.93 (d, *J* = 8.0 Hz, 2H), 5.14 (ddd, *J* = 15.7, 9.5, 6.4 Hz, 2H), 5.02 – 4.80 (m, 2H), 3.74 (s, 6H), 3.49 (q, *J* = 5.9 Hz, 4H).

^{13}C NMR (100 MHz, Acetonitrile-d_3) δ = 160.59, 158.44, 150.49, 143.10, 138.07, 137.81, 137.48, 124.72, 123.13, 113.98, 108.47, 106.09, 104.04, 56.49, 50.18, 34.83.

^{19}F NMR (376 MHz, Acetonitrile-d_3) δ = -151.82 (dd, *J* = 12.5, 7.3 Hz).

HRMS(ESI): *m/z*=Calcd for $C_{35}H_{31}N_4O_2^+$ $[M]^+$ 539.2442, found 539.2425

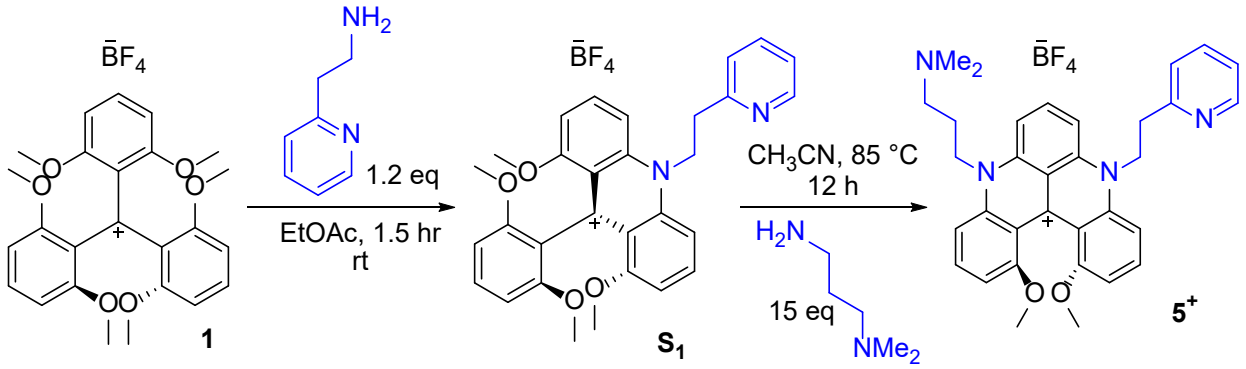

Racemic-5-(3-(dimethylamino)propyl)-1,13-dimethoxy-9-(2-(pyridin-2-yl)ethyl)-5,9-dihydro-13b*H*-quinolino[2,3,4-*kl*]acridin-13b-ylium tetrafluoroborate salt (5^+): 2-(pyridin-2-yl)ethan-1-amine (0.292 mg, 2.3 mmol, 1.2 equiv) was added to a solution of tris(2,6 dimethoxyphenyl)carbenium tetrafluoroborate (1.00 g, 1.99 mmol, 1.0 equiv) in anhydrous EtOAc (25 ml). The reaction mixture was stirred at room temperature for 1.5 hours. The crude product precipitated upon addition of hexane (~100 ml). The precipitate was filtered and washed several times with hexane and collected. Selective precipitation by addition of hexane to a solution of the crude product in CH_2Cl_2 afforded the 9-(2,6-dimethoxyphenyl)-1,8-dimethoxy-10-(2-(pyridin-2-yl)ethyl)-9,10-dihydroacridin-9-ylium tetrafluoroborate salts (**S1**, 1.07 g, 95%).[2] The first step product (1.0 g, 1.76 mmol, 1.0 equiv) was dissolved in anhydrous CH_3CN (15ml) and N,N-dimethylpropane-1,3-diamine (3.3 ml, 26.40 mmol, 15 equiv) was added. The reaction mixture was heated at 85 °C for 12 hours and then allowed to cool to room temperature. The crude product precipitated upon addition of Et_2O (~100 ml). The precipitate was filtered and washed several times with Et_2O and collected. Selective precipitation by addition of diethyl ether to a solution of the crude product in CH3CN afforded the dimethoxyquinacridinium tetrafluoroborate salts (0.94 g, 88%).

Grey solid; Melting point: 218-220 °C; R_f= 0.30 (SiO_2, CH_2Cl_2:MeOH (80:20));

^{1}H NMR (400 MHz, Chloroform-*d*) δ = 8.67 – 8.51 (m, 1H), 8.24 (t, *J* = 8.5 Hz, 1H), 7.91 (ddd, *J* = 8.9, 8.0, 6.9 Hz, 2H), 7.76 (d, *J* = 8.5 Hz, 1H), 7.69 (td, *J* = 7.7, 1.9 Hz, 1H), 7.63 (t, *J* = 8.6 Hz, 2H), 7.53 (d, *J* = 8.9 Hz, 1H), 7.44 (d, *J* = 7.7 Hz, 1H), 7.22 (ddd, *J* = 7.6, 4.8, 1.1 Hz, 1H), 6.86 (dd, *J* = 8.0, 2.1 Hz, 2H), 5.12 (ddd, *J* = 15.8, 9.7, 6.7 Hz, 1H), 4.90 (ddd, *J* = 15.5, 9.7, 6.5 Hz, 1H), 4.81 (ddd, *J* = 15.5, 9.8, 6.0 Hz, 1H), 4.62 (ddd, *J* = 15.4, 9.8, 5.9 Hz, 1H), 3.77 (s, 3H), 3.76 (s, 3H), 3.53 (td, *J* = 6.2, 3.0 Hz, 2H), 2.58 (t, *J* = 6.3 Hz, 2H), 2.35 (s, 6H), 2.28 – 2.10 (m, 1H).

13C NMR (100 MHz, Chloroform-*d*) δ = 159.78, 156.98, 149.82, 142.94, 142.20, 142.14, 138.97, 138.82, 137.73, 137.58, 137,32, 137.17, 124.18, 122.48, 119.23, 113.34, 107.47, 107.40, 105.17, 105.07, 103.22, 103.11, 56.44, 55.83, 45.78, 34.39, 24.82.

^{19}F NMR (376 MHz, Chloroform-*d*)) δ = -151.90 (d, *J* = 20.3 Hz).

HRMS(ESI): *m/z*=Calcd for $C_{33}H_{35}N_4O_2^+$ $[M]^+$ 519.2755, found 519.2743.

II.2 Typical Procedure for synthesis of 2-H•, 2-NO$_2$•, and 3• - 5•

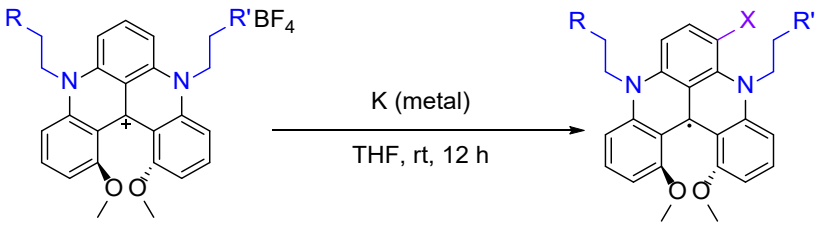

2-H•, R=R'= -CH_2NMe_2, X = H, 82%,
2-NO$_2$•, R=R'= -CH_2NMe_2, X= NO_2, 80%,
3•, R=R'= -pyridyl, X = H, 80%,
4•, R=R'= -CH_3, X = H, 75%,
5•, R = -CH_2NMe_2, R' = -pyridyl, X = H, 86%

The potassium metal[3][4] (1.1 equiv) was added to the stirred solution of dimethoxyquinacridinium tetrafluoroborate salts (200 mg, 1 equiv) in anhydrous THF (10 ml). The reaction mixture was stirred at rt for 12 hours and then reaction mixture was filtered and evaporated under vacuum pump. The crude product was triturated 2 times in 5 mL of Et_2O then extract with toluene and filtrated again. The filtrate was recrystallized from toluene and hexane layering to afford the radical **2•-5•**.

Paramagnetic NMR spectrums were obtained in C_6D_6 and the spectra are visible in what follows (Figures S14-15). Due to the important paramagnetic character paramagnetic character demonstrated by these species, the complete H attribution could not be completed.

HRMS(ESI) data for radicals:

2-H• : *m/z* = Calcd for $C_{31}H_{39}N_4O_2$: 499.3068, found 499.3068.

2-NO$_2$• : *m/z* = Calcd for $C_{31}H_{38}N_5O_4$: 544.2918, found 519.2893.

3• : *m/z* = Calcd for $C_{33}H_{35}N_4O_2$: 519.2755, found 519.2743.

4• : *m/z* = Calcd for $C_{35}H_{31}N_4O_4$: 539.2442, found 539.2443.

5• : *m/z* = Calcd for $C_{33}H_{35}N_4O_2$: 519.2755, found 519.2743.

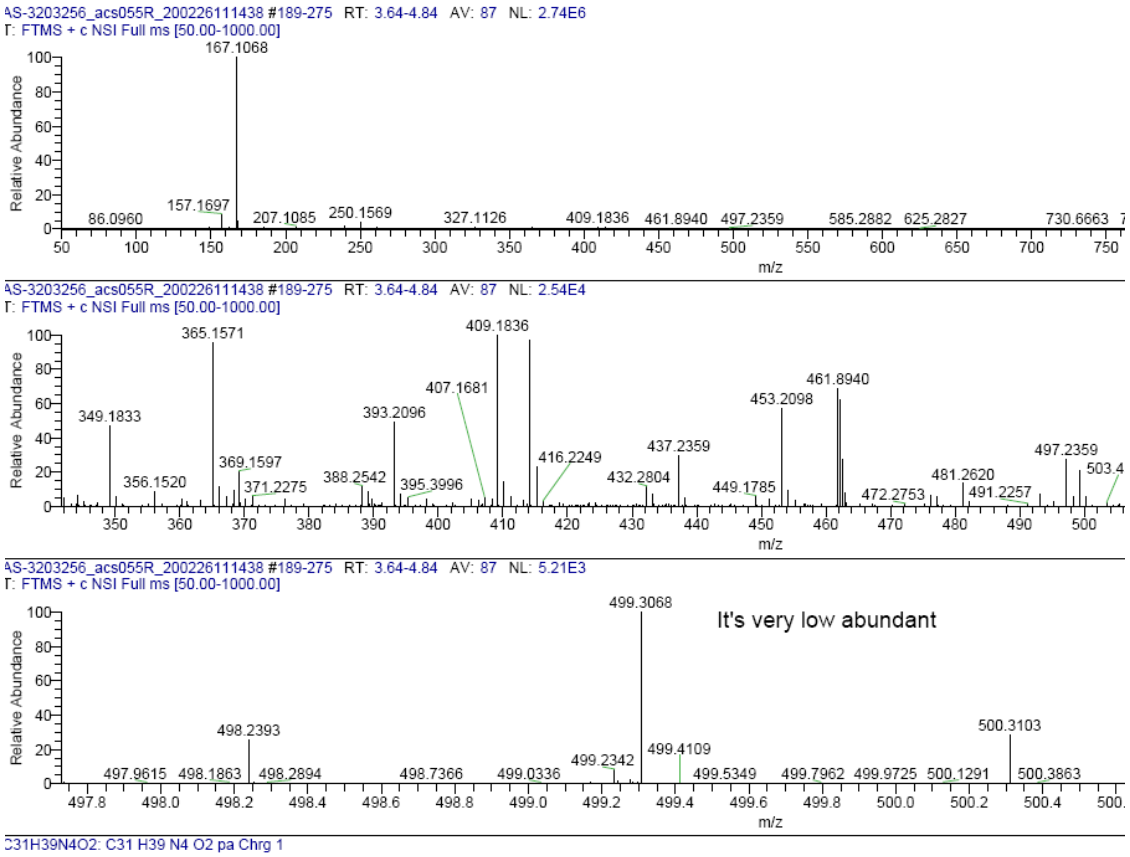

Figure S1. HRMS (ESI) spectra of **2-H•**

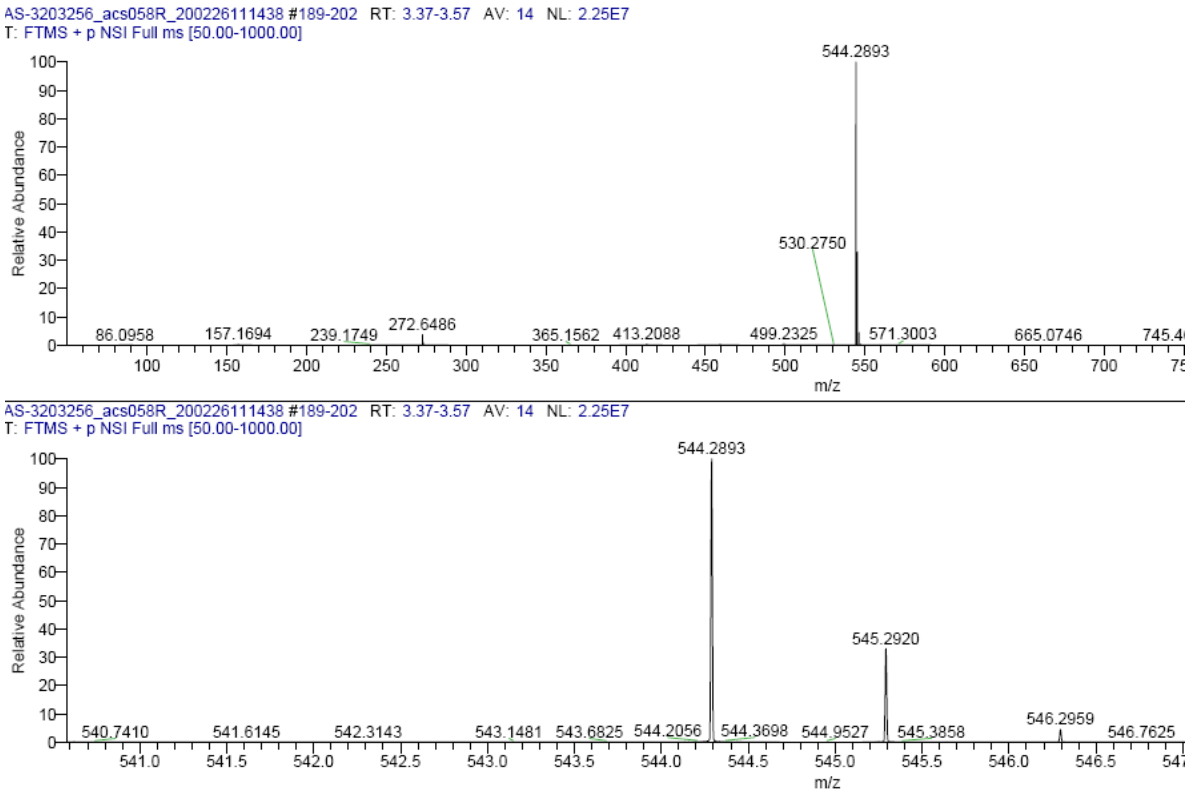

Figure S2. HRMS (ESI) spectra of **2-NO_2•**

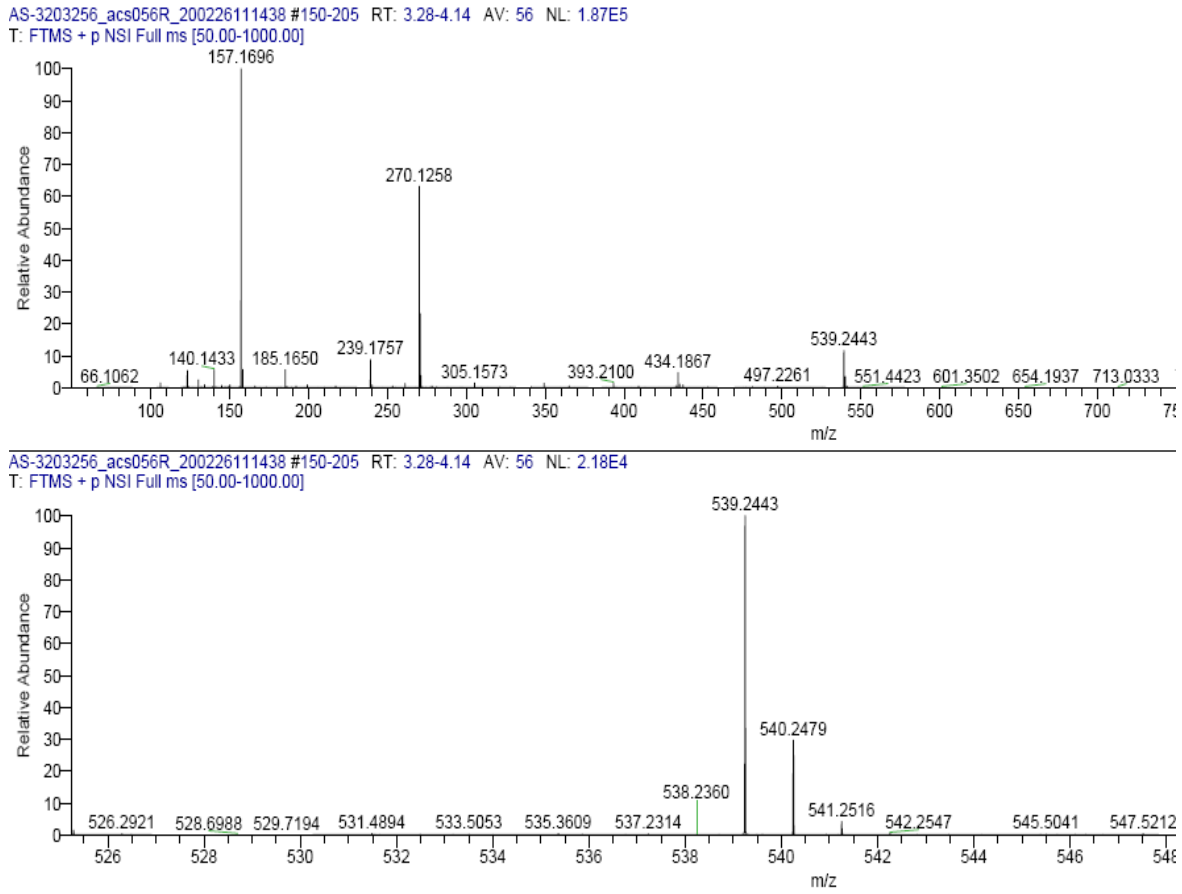

Figure S3. HRMS (ESI) spectrum of **3˙**

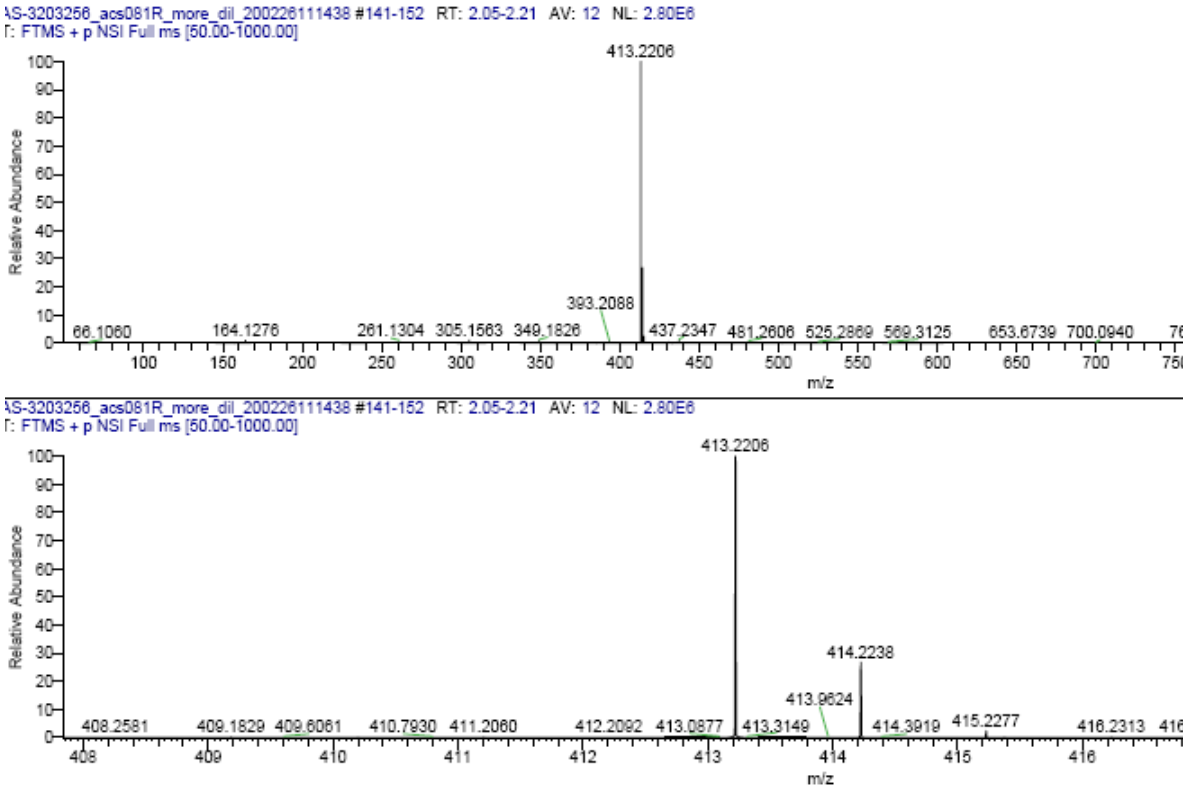

Figure S4. HRMS (ESI) spectra of **4˙**

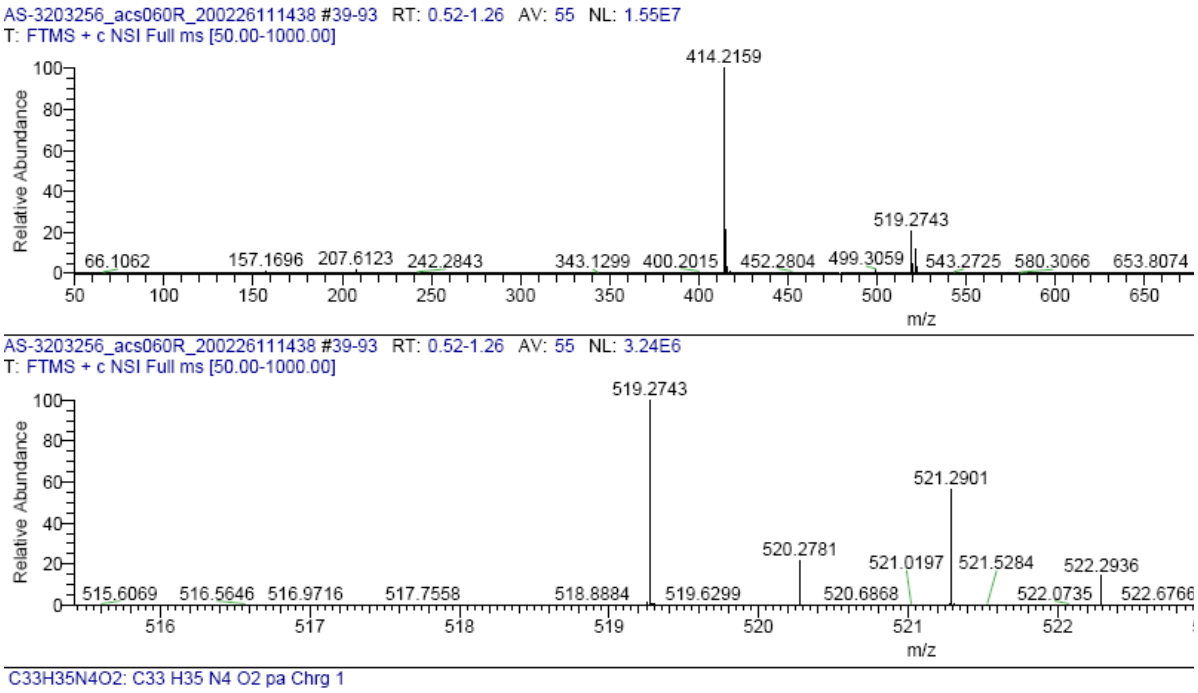

Figure S5. HRMS (ESI) spectraof **5**•

III. NMR Spectroscopy data

III.1 NMR spectra of carbenium 2-H⁺

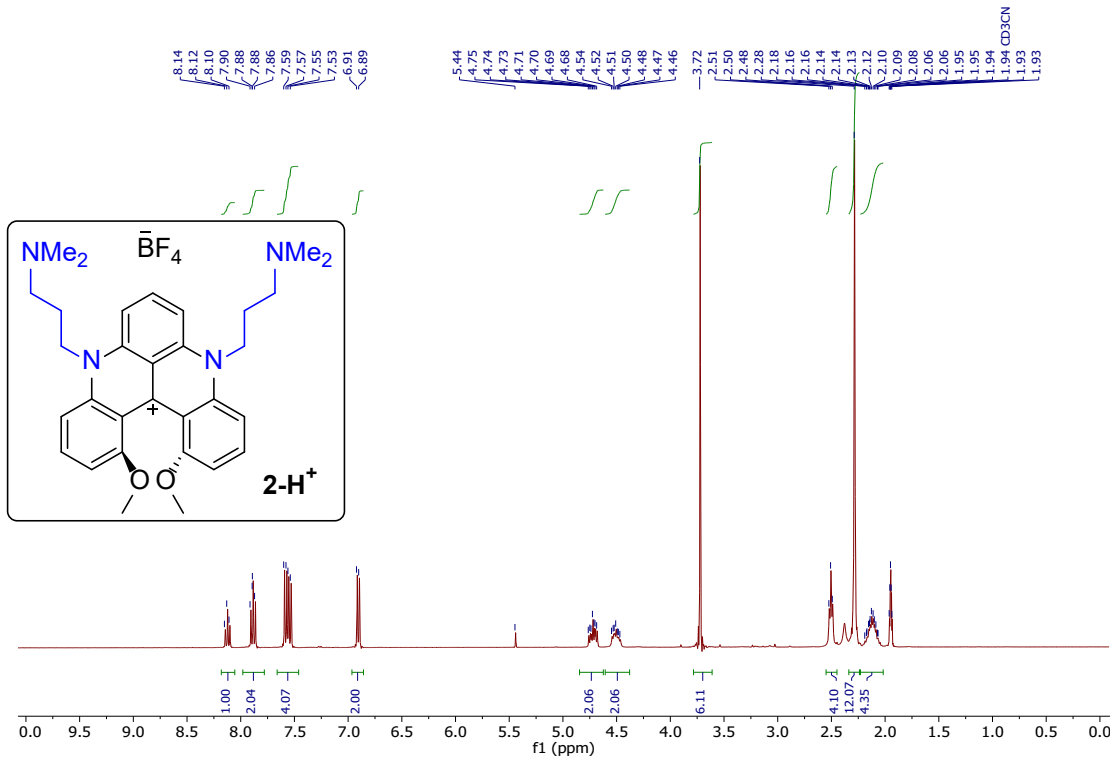

Figure S6. ^{1}H NMR spectrum of **2**$^{+}$ in CD_3CN

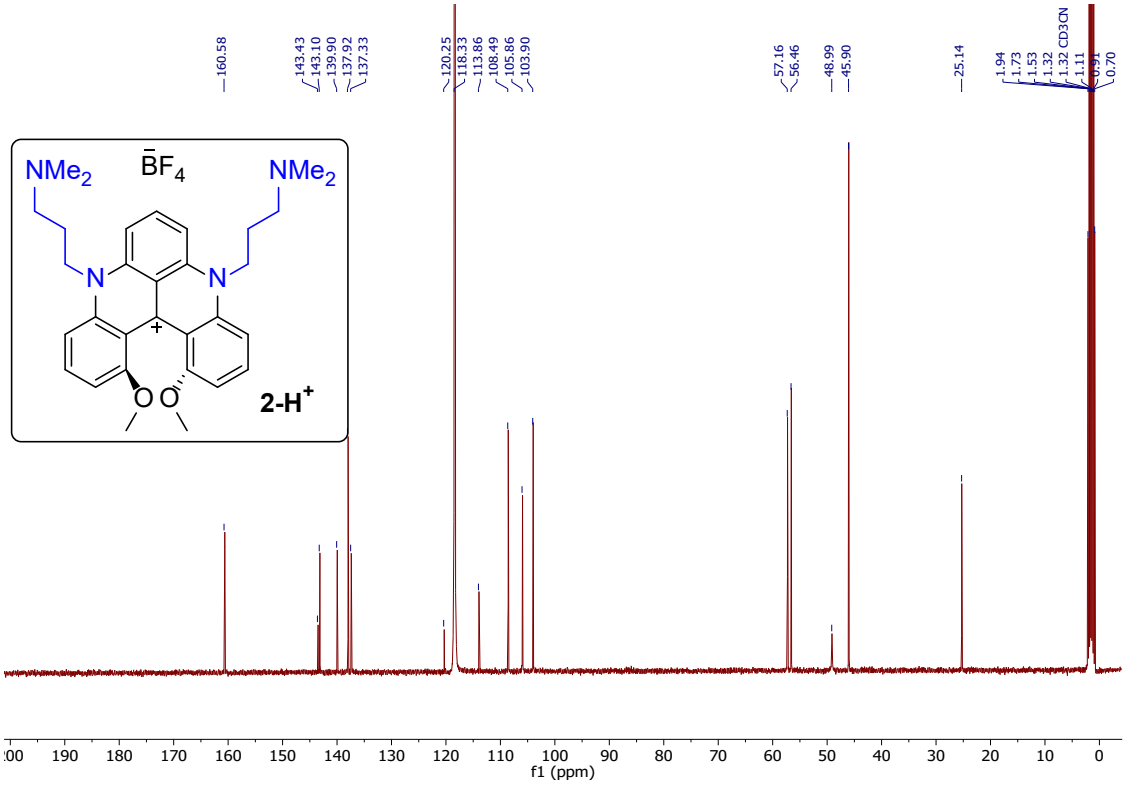

Figure S7. ^{13}C NMR spectrum of **2-H**$^{+}$ in CD_3CN

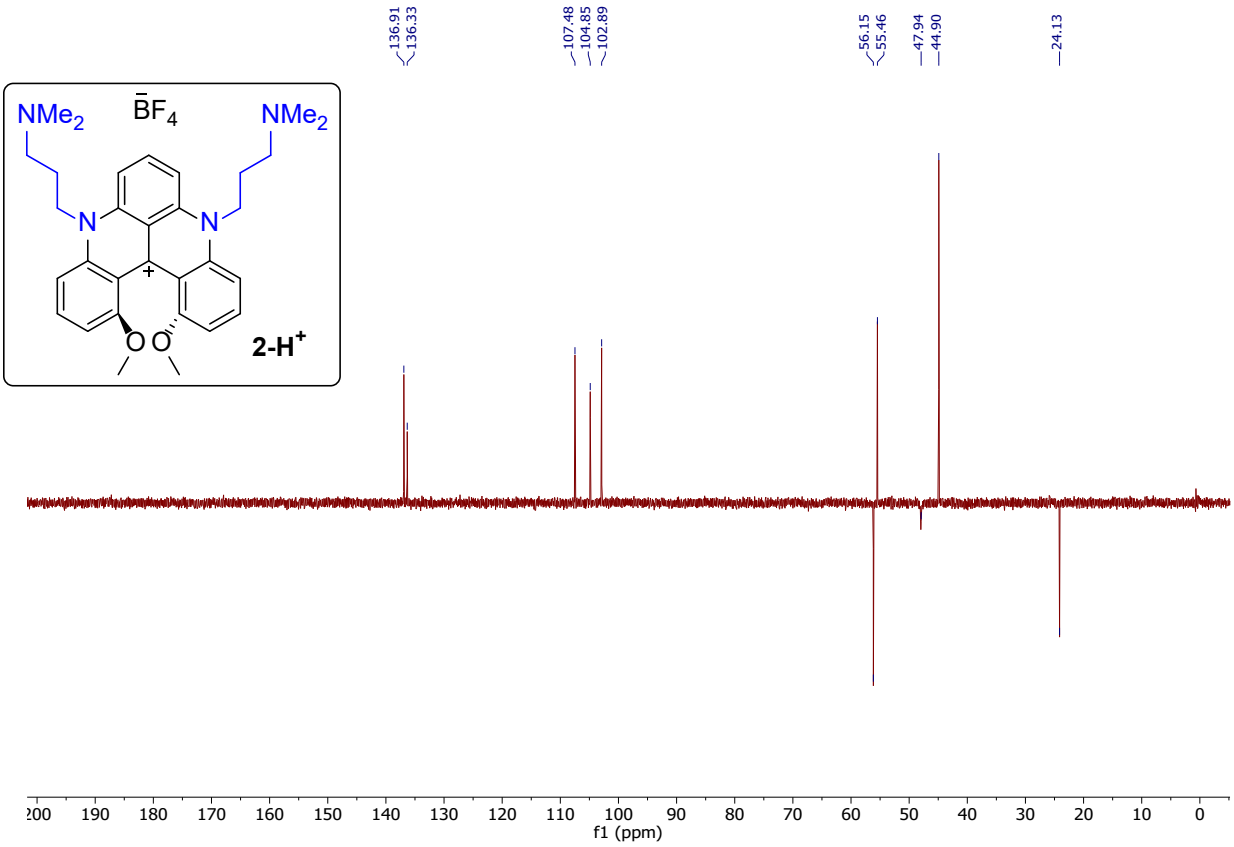

Figure S8. ^{13}C DEPT-135 NMR spectrum of **2-H**$^{+}$ in CD_3CN

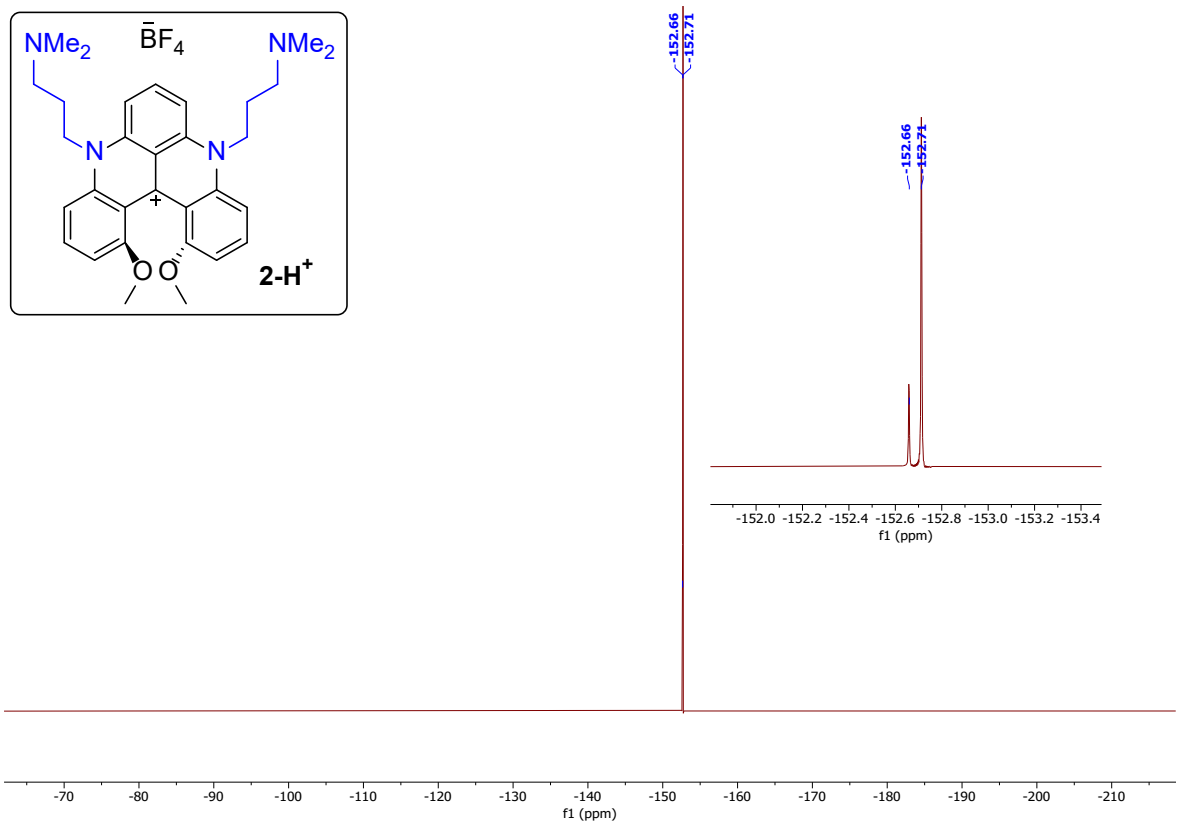

Figure S9. ^{19}F NMR spectrum of **2-H**$^{+}$ in CD_3CN

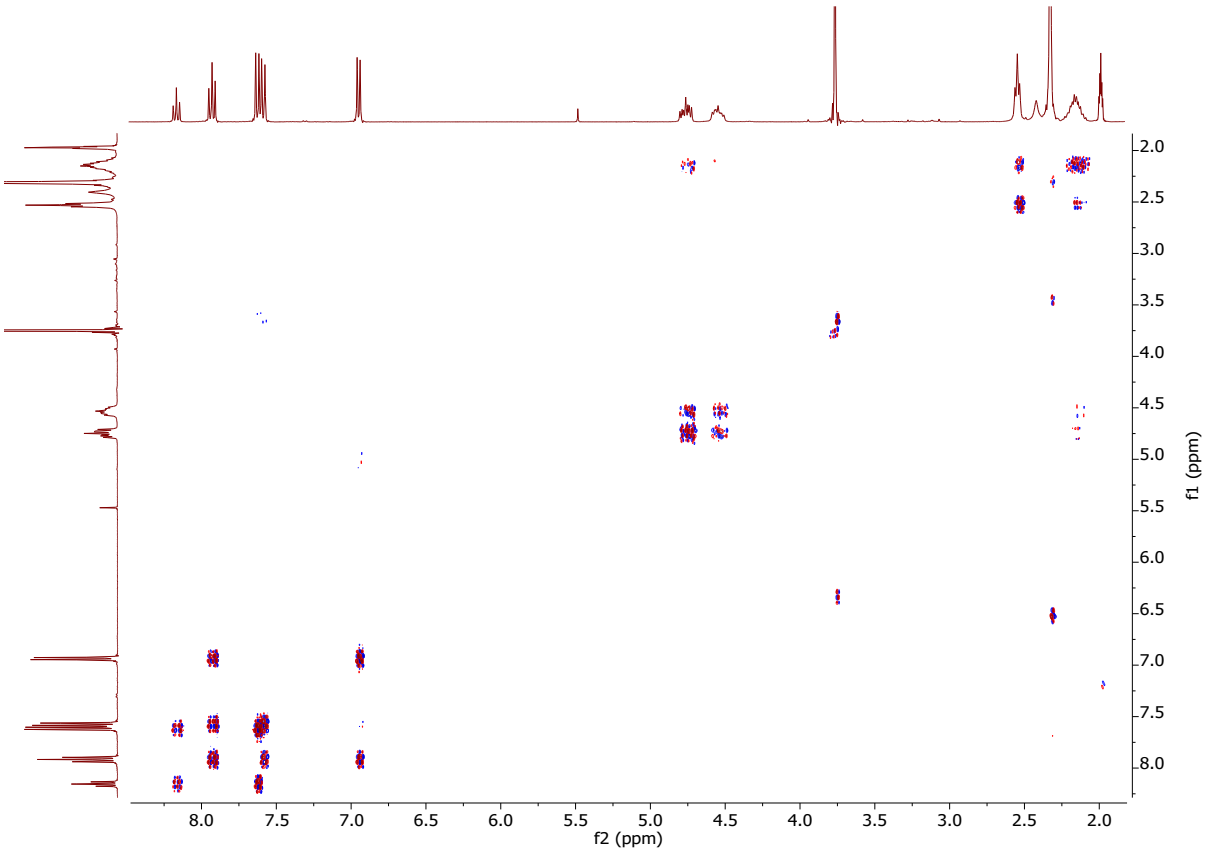

Figure S10. ^{1}H-^{1}H COSY spectrum of **2-H**$^{+}$ in CD_3CN

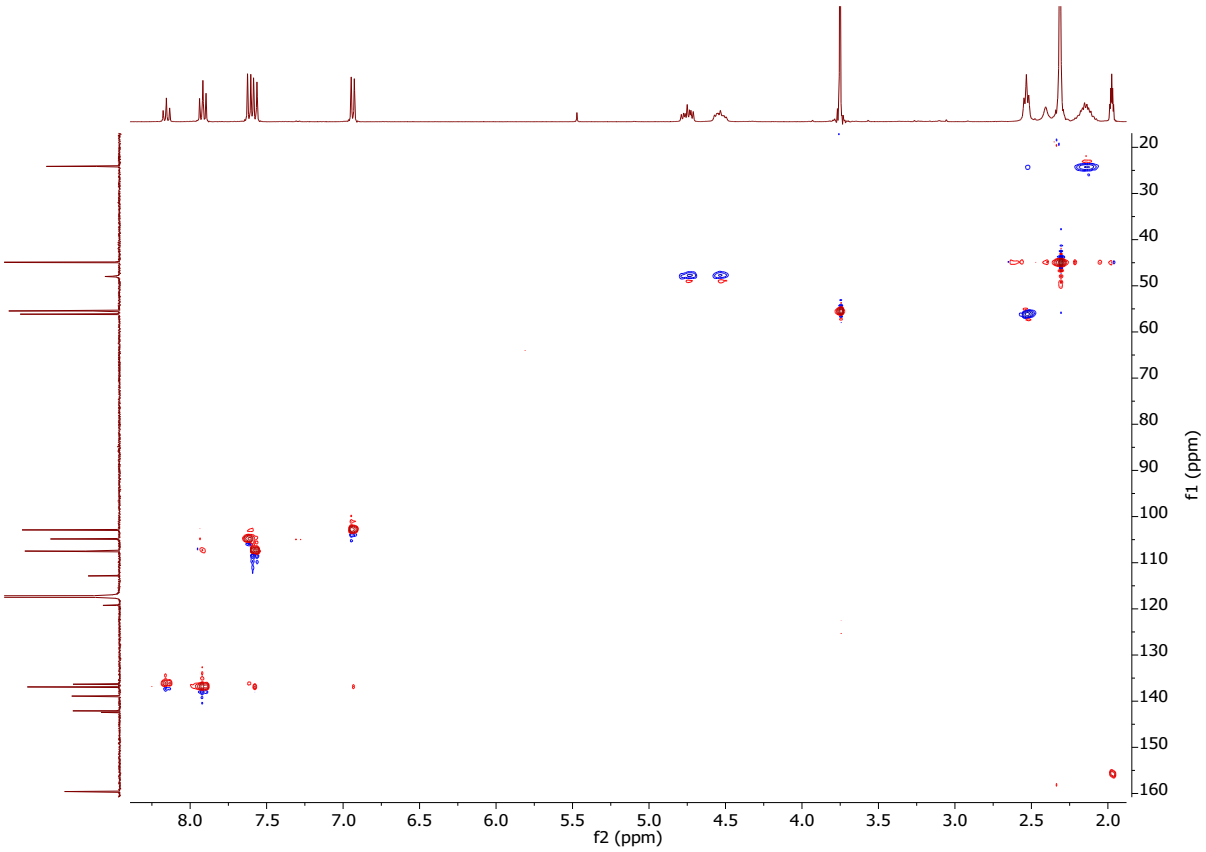

Figure S11. ^{1}H-^{13}C HMBC spectrum of **2-H**$^{+}$ in CD_3CN

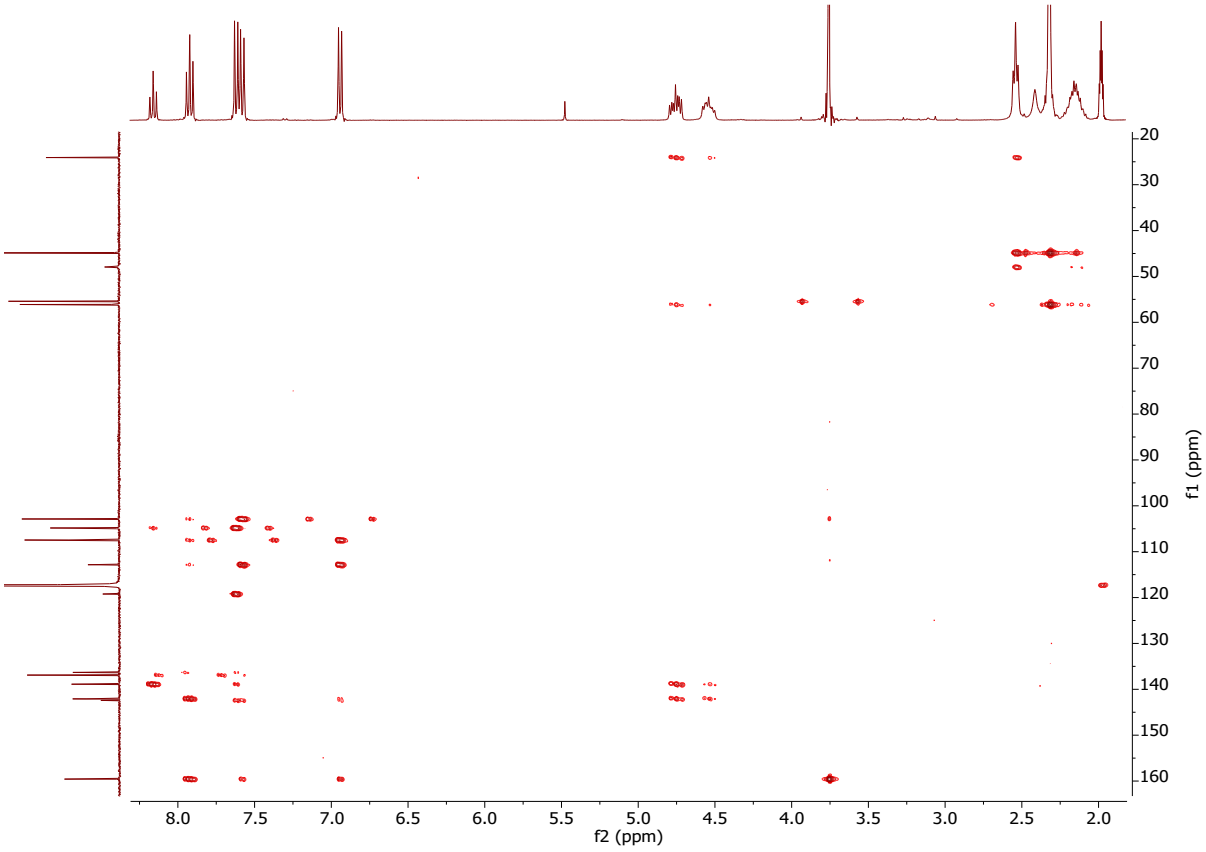

Figure S12. ^{1}H-^{13}C HSQC spectrum of **2-H**$^{+}$ in CD_3CN

III.2 NMR spectra of carbenium 2-NO_2^+

The carbenium **2-NO_2^+** has an unresolved ^{1}H NMR spectrum in CD_2Cl_2 at room temperature. Variable temperature (VT) ^{1}H NMR spectroscopy analysis of **2-NO_2^+** was conducted to resolve the broad signals observed. The sample was prepared in a non-coordinating deuterated dichloromethane and studied over a temperature range of 333 – 193 K (see Figures S13-S14). At room temperature (293 K), ^{1}H NMR spectrum shows that the aromatic protons are poorly resolved, and the amino arms are in a rapid exchange suggested by the broad signal at 4.94 ppm. Decreasing the temperature to 193 K results in a sharp and well-defined proton signals (See Figure S15). The presence of the NO_2 group result in a low symmetry molecule as exemplified by the aromatic region, the two signals for OMe groups (at 3.77 and 3.73 ppm), two signals for NMe2 groups (2.32 and 1.40 ppm). The assignment of the six methylenic protons of the -*n*Pr-NMe_2 arms was successfully carried out using low-temperature ^{1}H-^{1}H COSY NMR sequence (see Figure S17). As observed in **2-H^+**, the two methylene groups alpha to helicenium scaffold are diasterotopic with the CH_2 near the NO_2 group resonating at 4.95/3.55 ppm (H_A/$H_{A'}$) and the other resonating at 4.86/4.68 ppm. However, instead of four additional freely rotating methylene groups (-CH_2(**CH_2)$_2$**NMe_2), we observed another set of diasterotopic methylenic protons at 1.92/1.75 ppm (H_B/$H_{B'}$). The presence of diastereostopic H_B/$H_{B'}$ protons along with the large chemical shift difference between the NMe_2 groups suggest an interaction between the nitrogen-lone pair of one -*n*Pr-NMe_2 arm and the C^+ carbocation center (Scheme S1). This interaction is further supported by the presence of a resolved ^{1}H NMR spectrum at room temperature for the reported **4-NO_2^+** compound containing -^{n}Pr arms instead of -*n*Pr-NMe_2.[3]

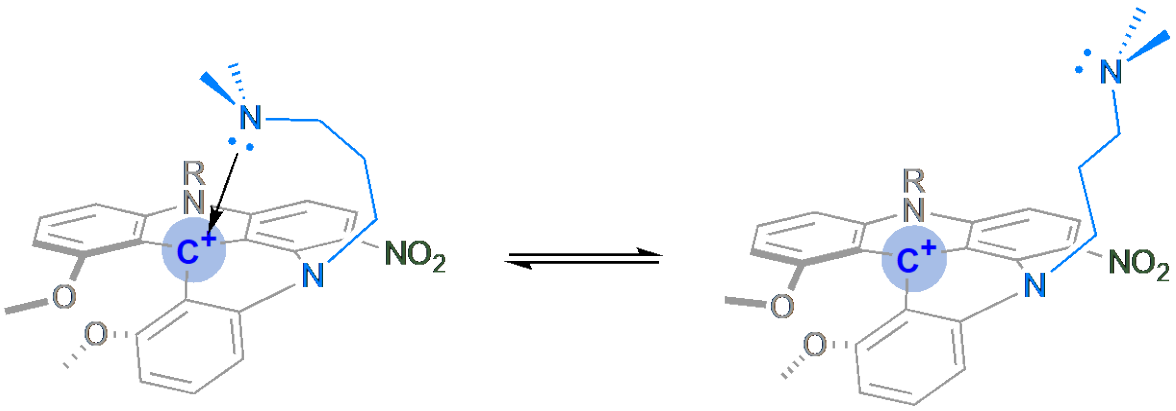

Scheme S1. NMe_2–C^+ interaction

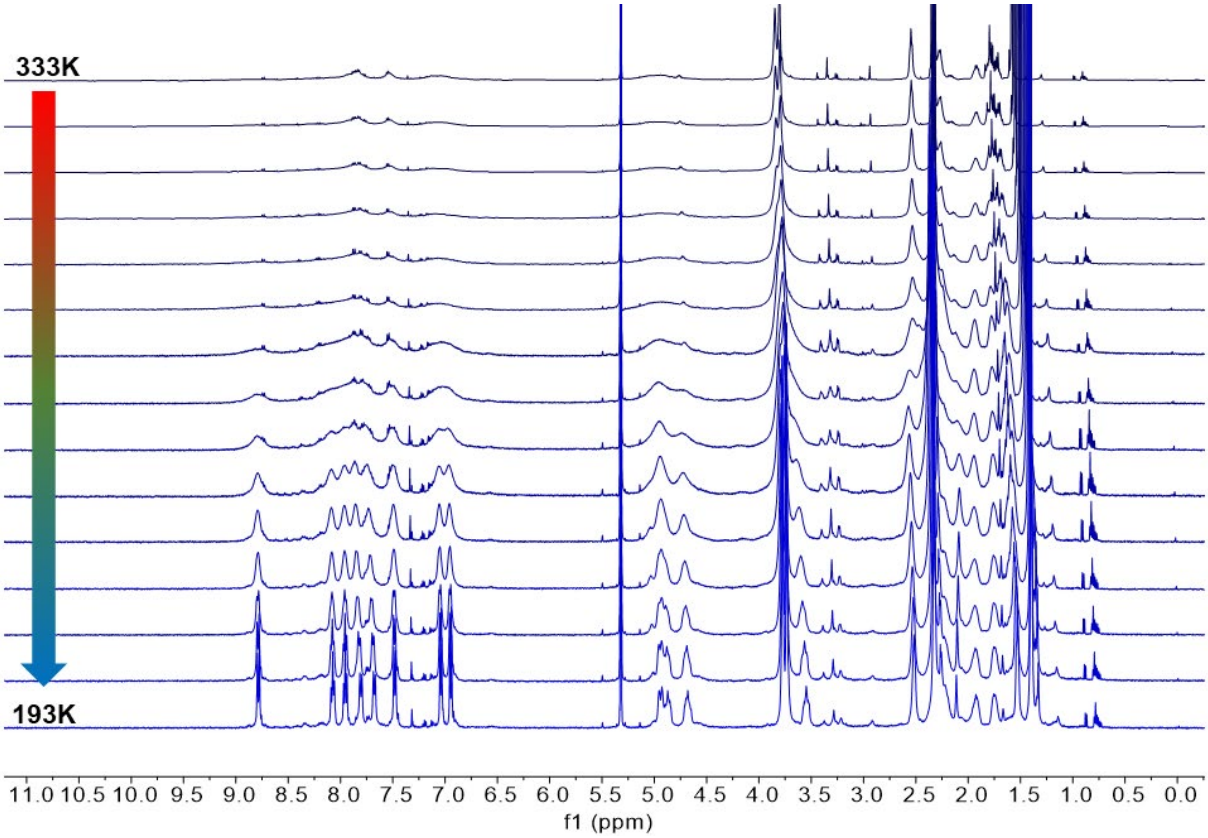

Figure S13 : ^{1}H NMR spectra of **2-NO$_2^+$** in CD_2Cl_2 between 333 K and 193 K with 10 K increments.

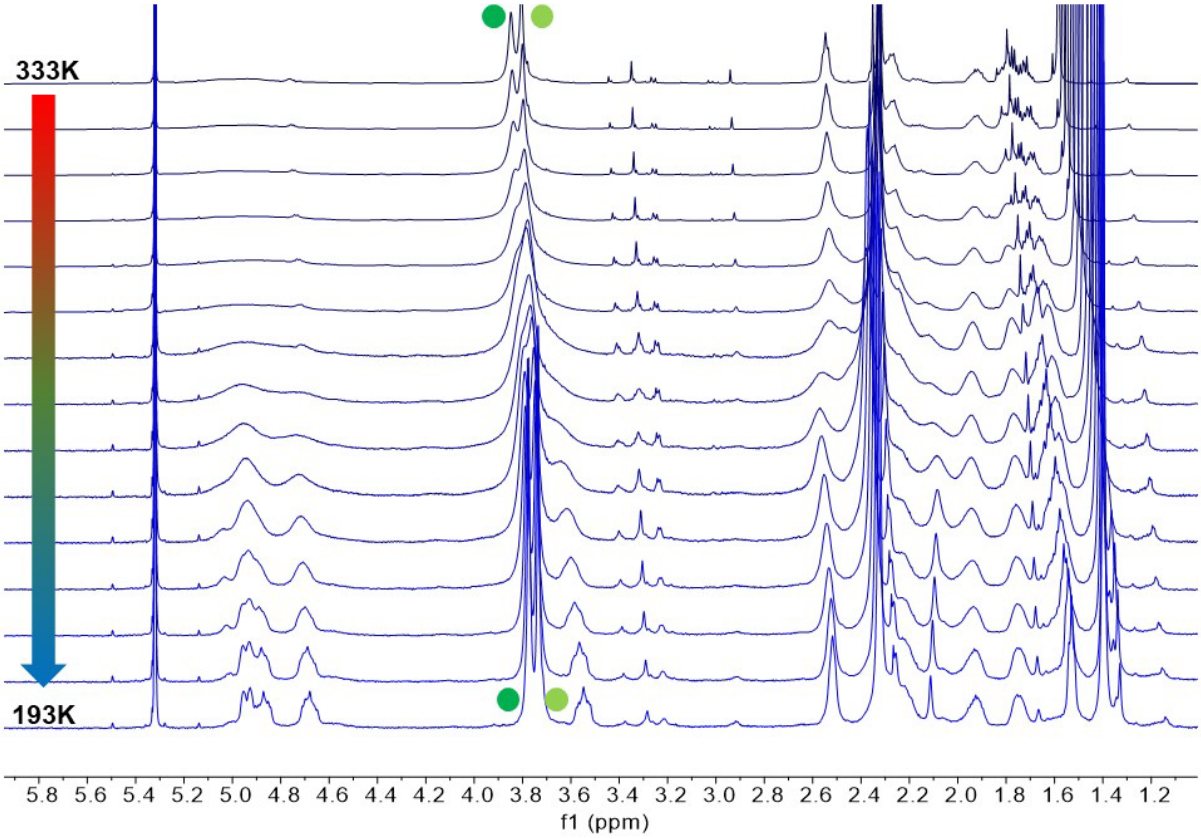

Figure S14 : ^{1}H NMR of **2-NO$_2^+$** in CD_2Cl_2 between 333 K and 193 K with 10 K increments.

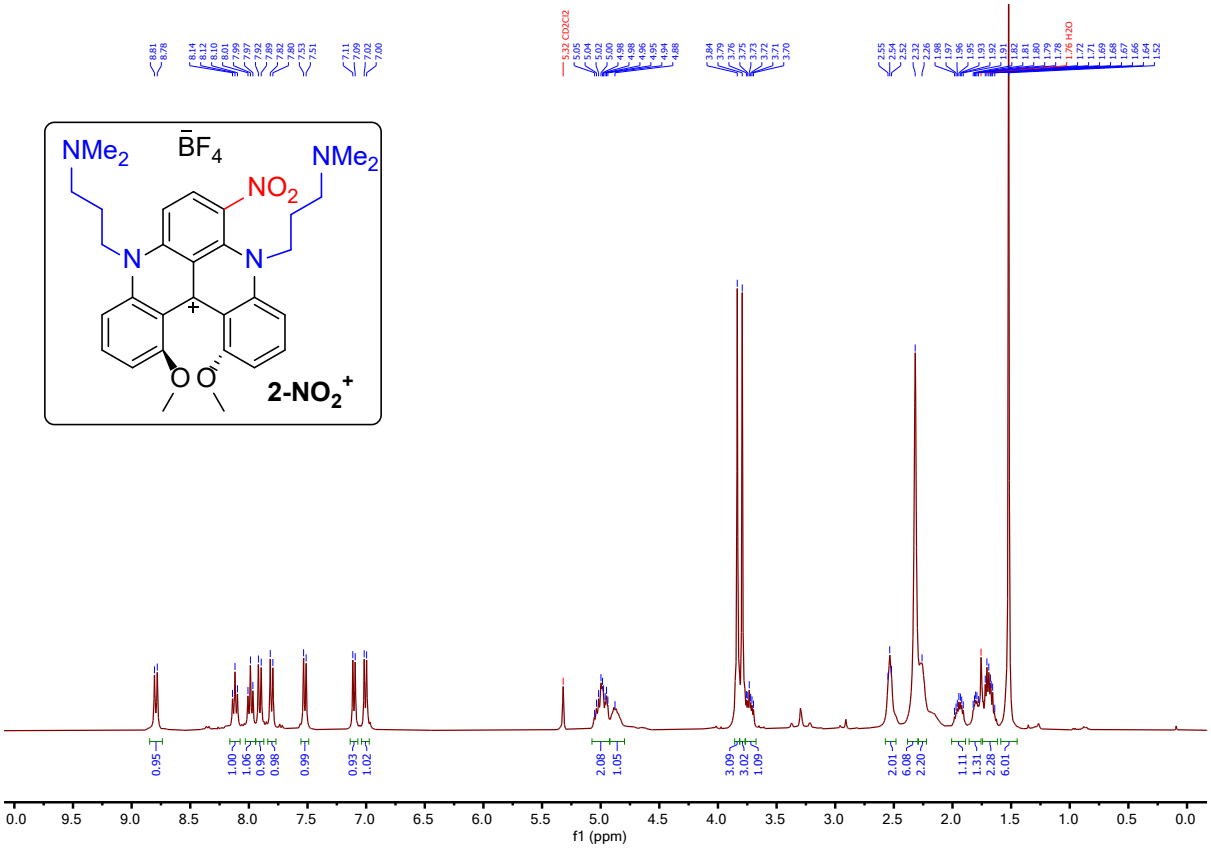

Figure S15: ^{1}H NMR of **2-NO_2^+** in CD_2Cl_2 at 193 K.

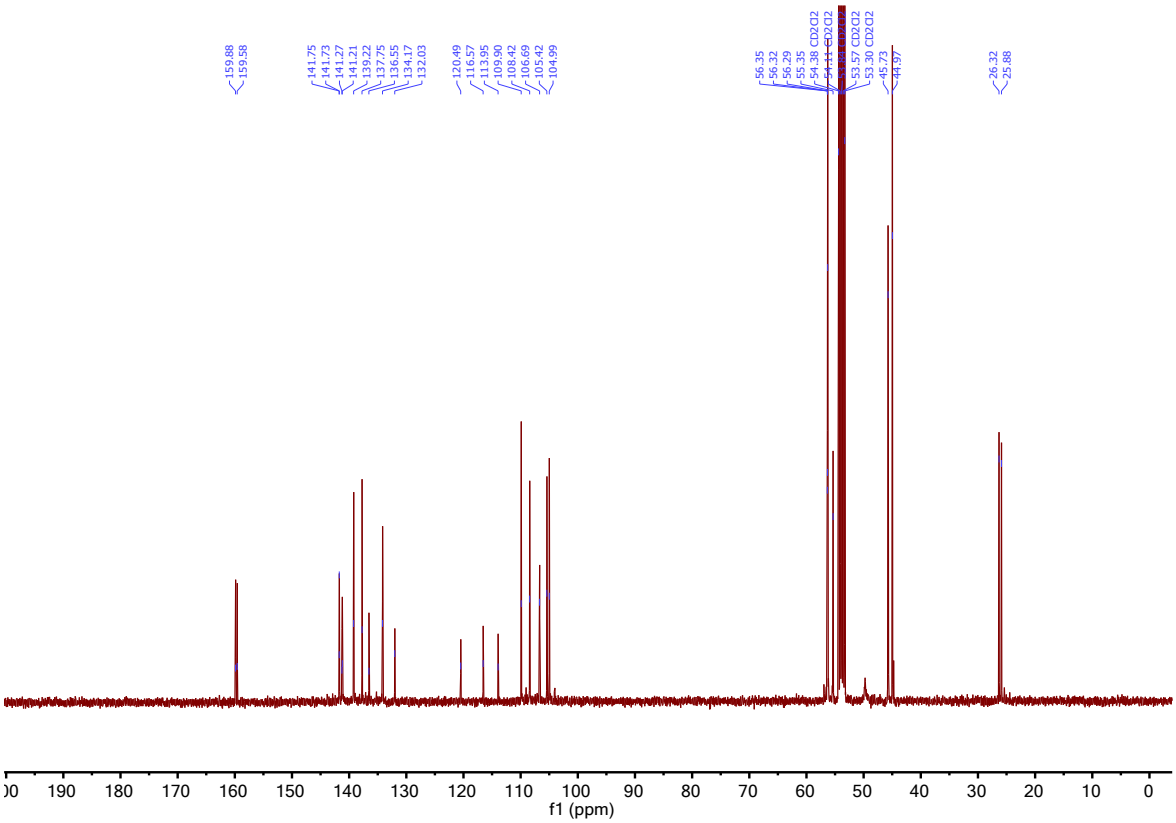

Figure S16. ^{13}C NMR spectrum of **2-NO_2^+** in CD_2Cl_2 at 193 K

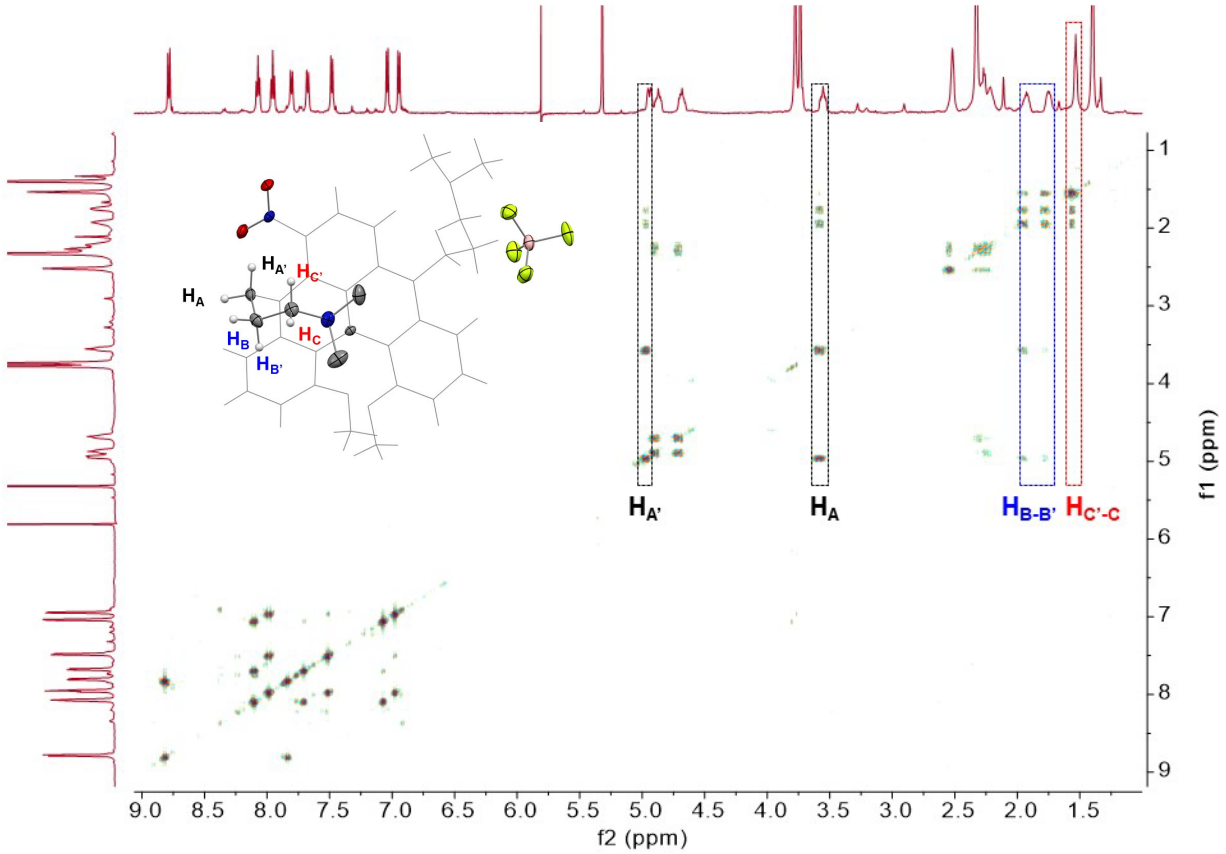

Figure S17: ^{1}H-^{1}HCOSY NMR spectrum of **2-NO$_2^+$** in CD_2Cl_2 at 200K and XRD attribution.

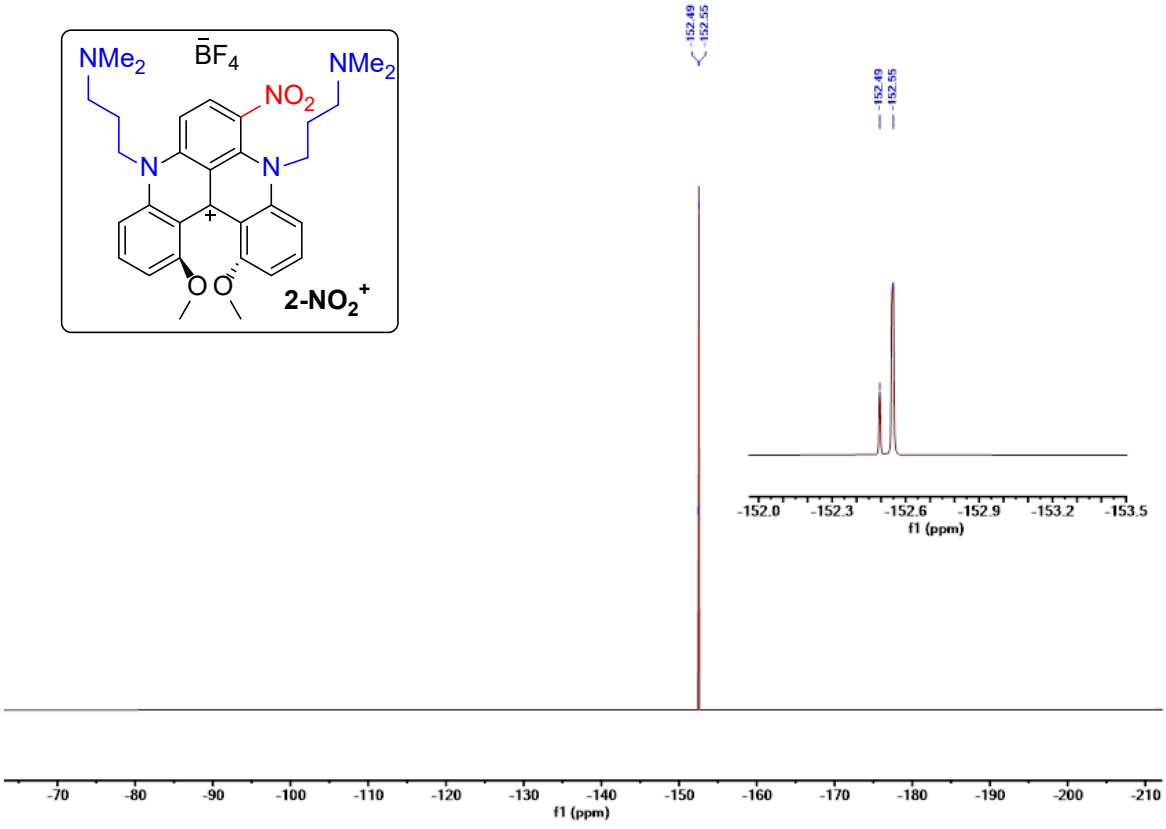

Figure S18: ^{19}F NMR spectrum of **2-NO$_2^+$** in CD_2Cl_2.

III.3 NMR spectra of carbenium 3^+ and 5^+

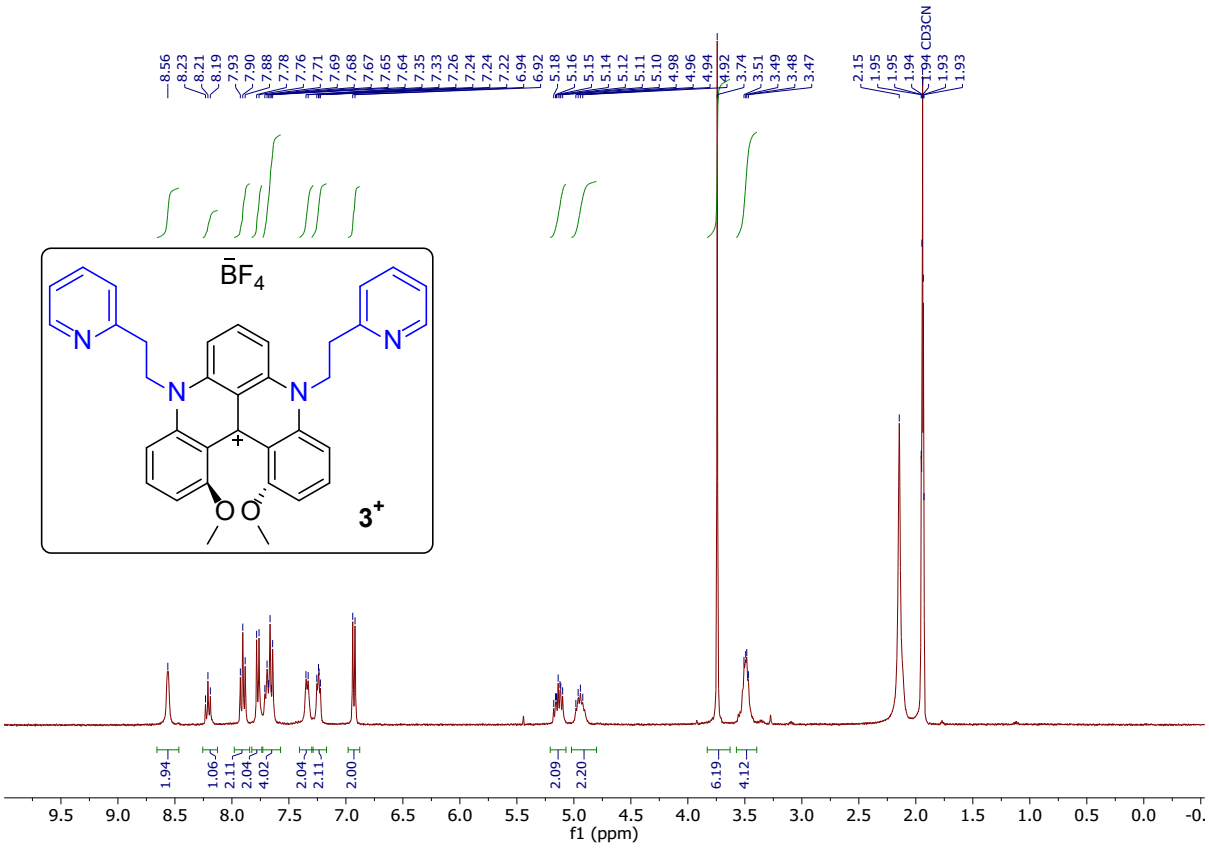

Figure S19. ^{1}H NMR spectrum of $\mathbf{3}^+$ in CD_3CN

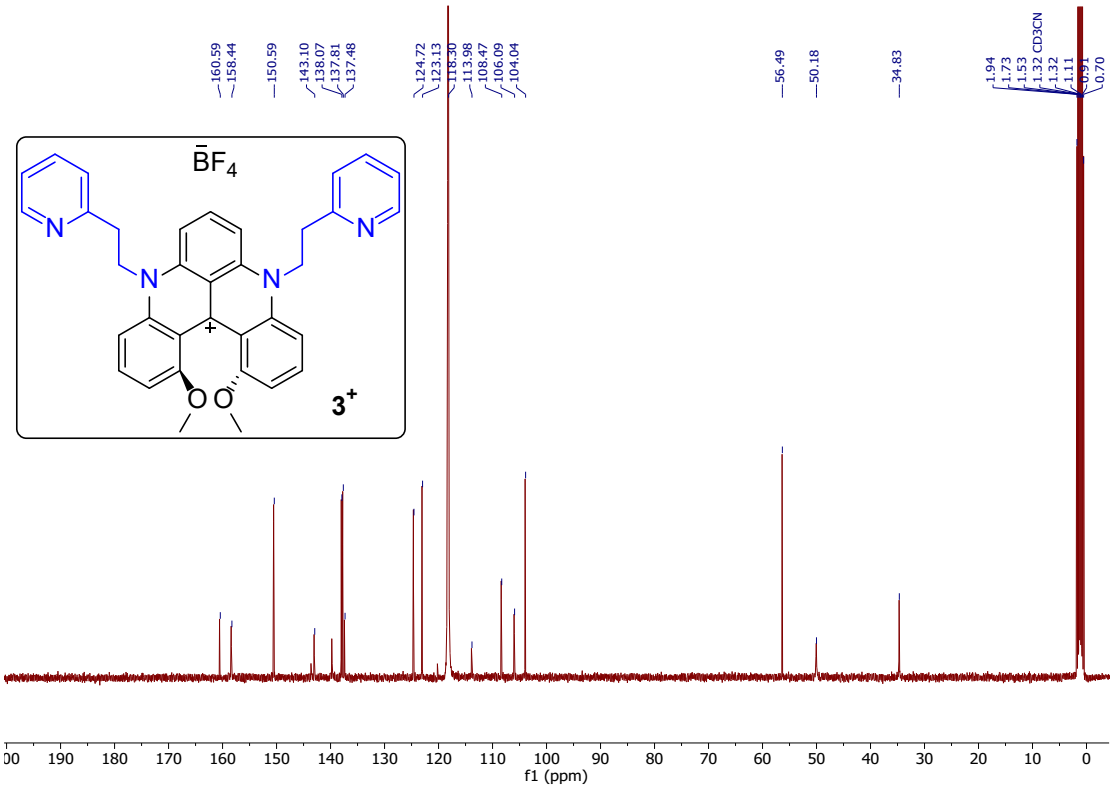

Figure S20. ^{13}C NMR spectrum of $\mathbf{3}^+$ in CD_3CN

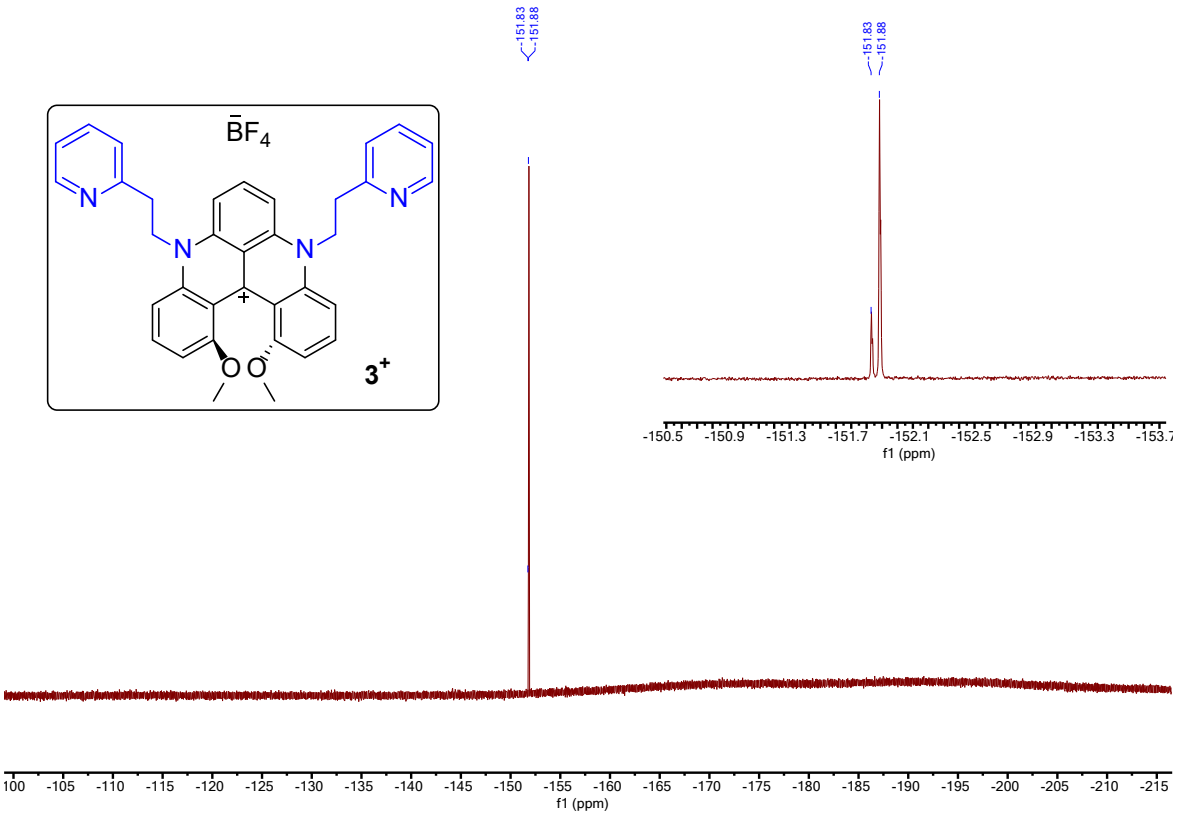

Figure S21. ^{19}F NMR spectrum of $\mathbf{3}^+$ in CD_3CN

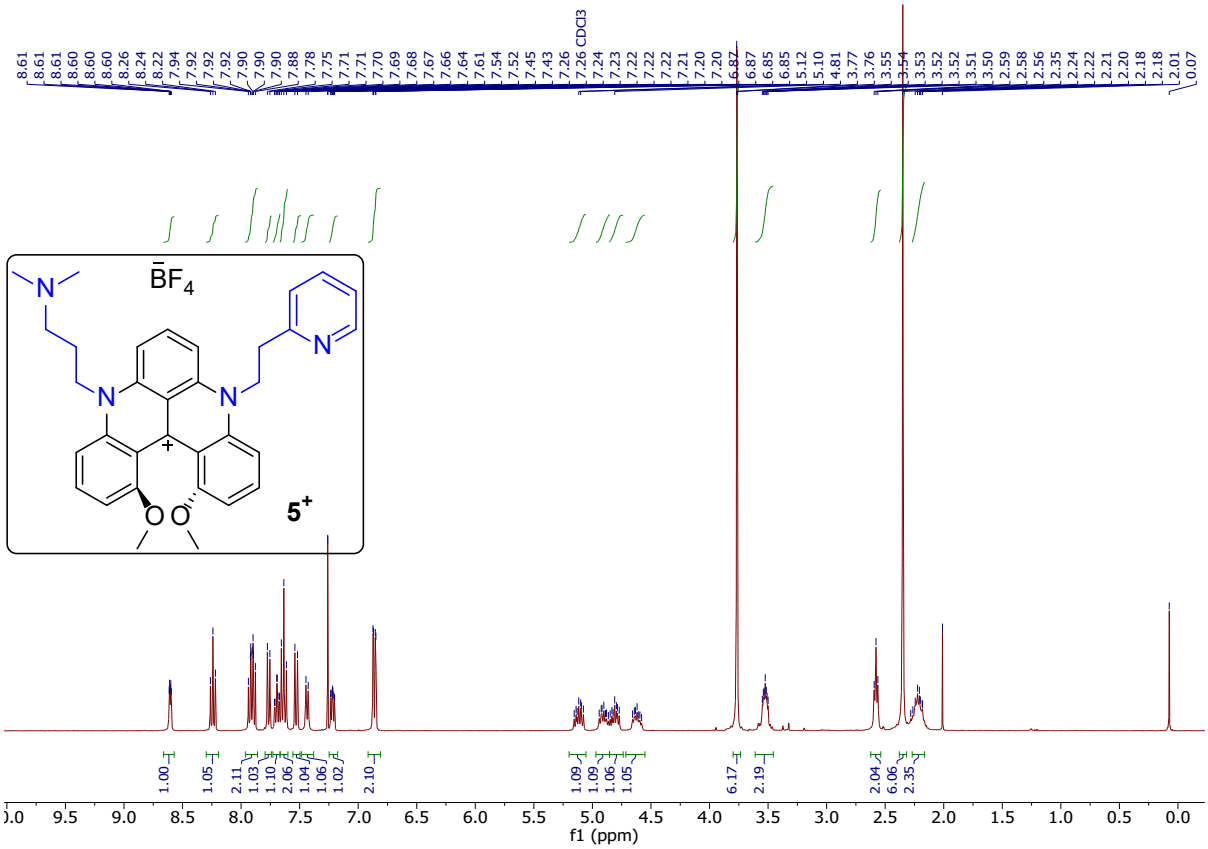

Figure S22. ^{1}H NMR spectrum of $\mathbf{5}^+$ in CD_3CN

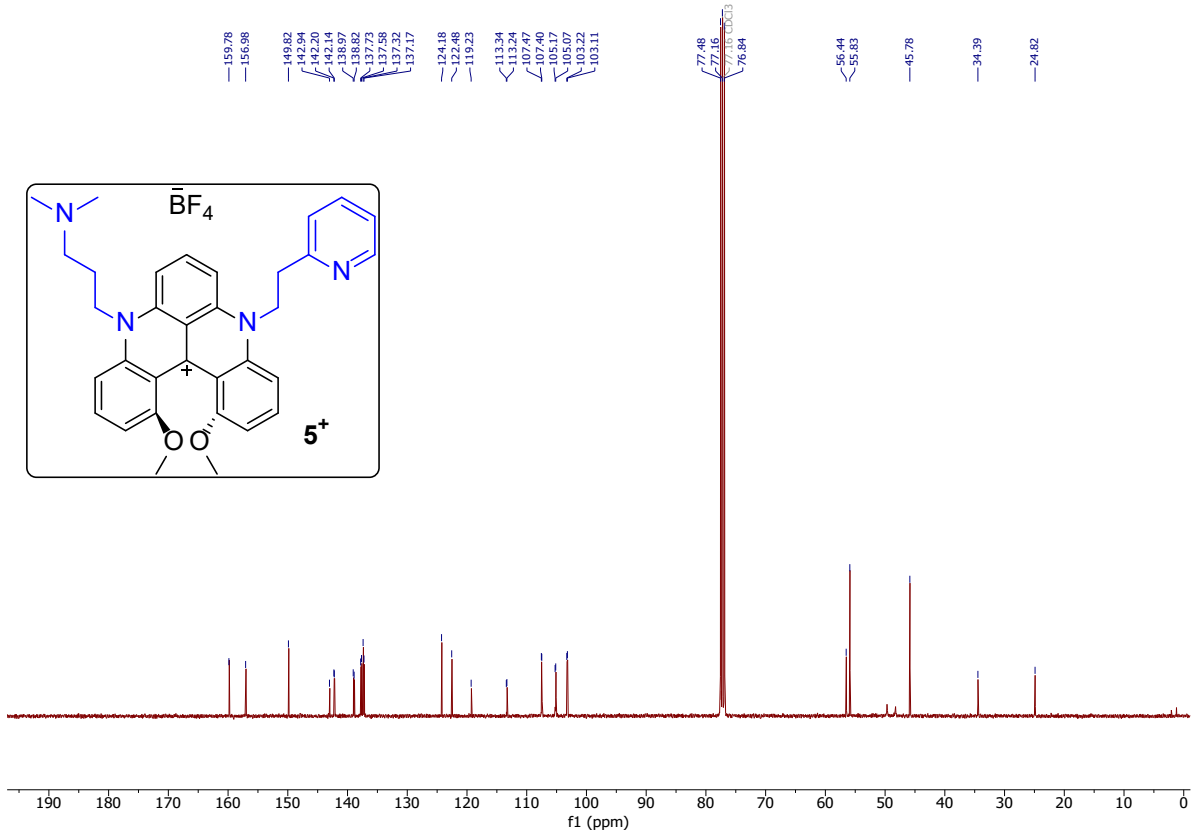

Figure S23. ^{13}C NMR spectrum of $\mathbf{5}^{+}$ in CD_3CN

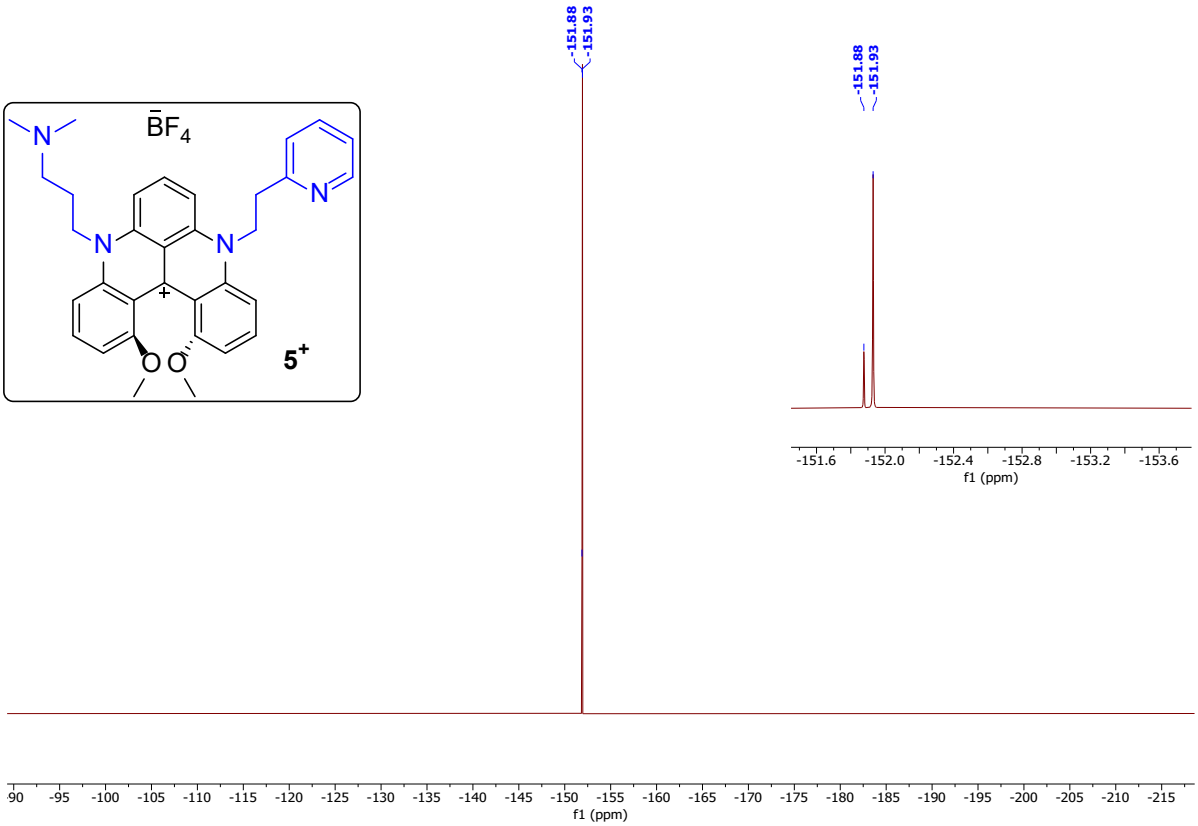

Figure S24. ^{19}F NMR spectrum of $\mathbf{5}^{+}$ in CD_3CN

III.3 NMR spectra of radical 2• - 5•

The molecules **2•-5•** were analyzed by paramagnetic ^{1}H NMR to determine if the pendant arms of the molecule have any effect or interaction with the radical system (see Figure S22-S23). The NMR sequence used to analyze these compounds had a window width of 100 ppm (SW = 100), a scan number of 256 (NS = 256) and a τ1 of 0.1 seconds (D1 = 0.1s).

Due to the pronounced radical nature of these compounds, the aromatic protons of the helicene radical scaffold are not observable However, the protons of the substituent arms *α* (N–***CH₂***–CH_2–R) and *β* (N–CH_2–***CH₂***–R) to the helicene core consistently appear broad and shifted at 17 and -7 ppm, respectively, for all radicals. The protons *γ* (N–CH_2–CH_2–***R***; R= C***H₃***, C***H₂***NMe_2, ***Py***) to the helicene core are less influenced by the radical, and while broad, resonate in the diamagnetic 10-0 ppm region. For **2-H•**, *γ*-protons as broad bands of 4 ppm wide centered around 5.71 ppm. The NO_2 electron-withdrawing group on **2-NO_2•** is speculated to have a widening effect on this band (from 9 to 2 ppm) still centered on around 5.71 ppm. The pyridinyl protons (*π*) for **3•** and **5•** are well-defined at 8.58, 7.38, 6.33 and 6.03 ppm respectively. In scaffold **5•**, the broad signature of *γ*-protons at 5.71 ppm is partially hidden by *π*-protons. The *γ*-protons on **4•** from the n-propyl groups are less affected by the radical system and appeared as a broad peak centered at 2.88 ppm. It thus appears that the nature of the chosen pendant arms has little influence on the radical character of the compounds **2•-5•**. Conversely, the substitution of a proton of the helicene core by an electron-withdrawing group induces a modification of the electronic structure of the resulting radical **2-NO_2•**.

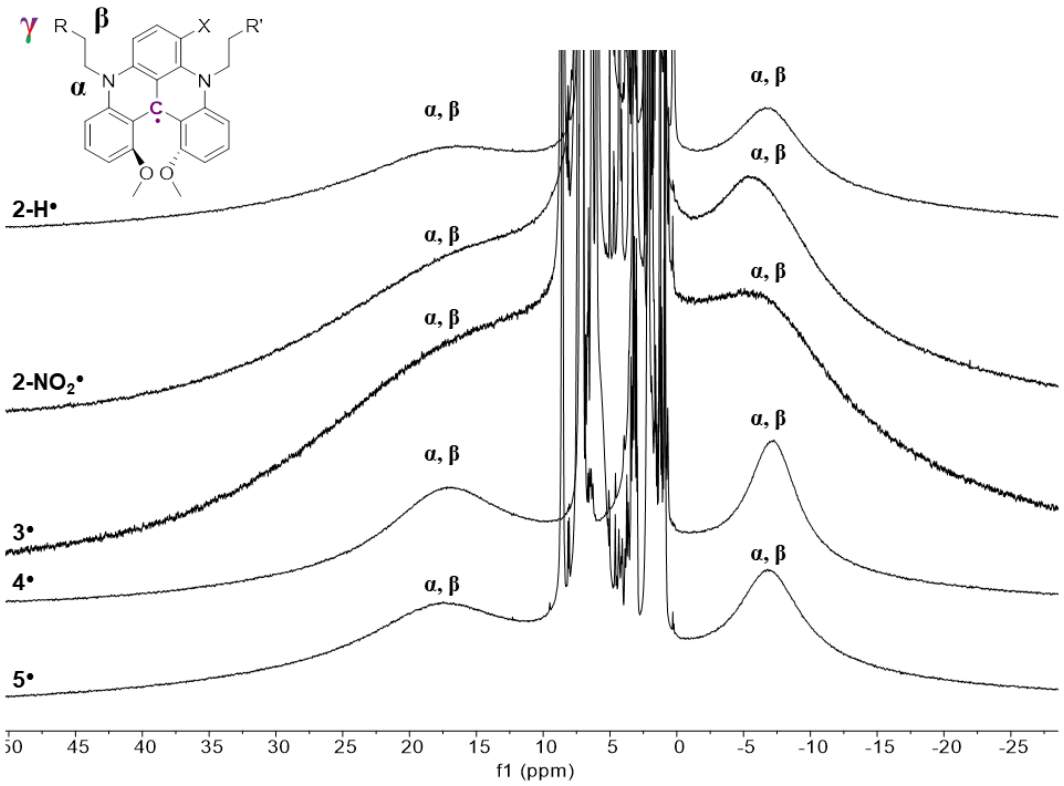

Figure S25 : ^{1}H NMR spectra of **2'-5'** in C_6D_6 at 298 K

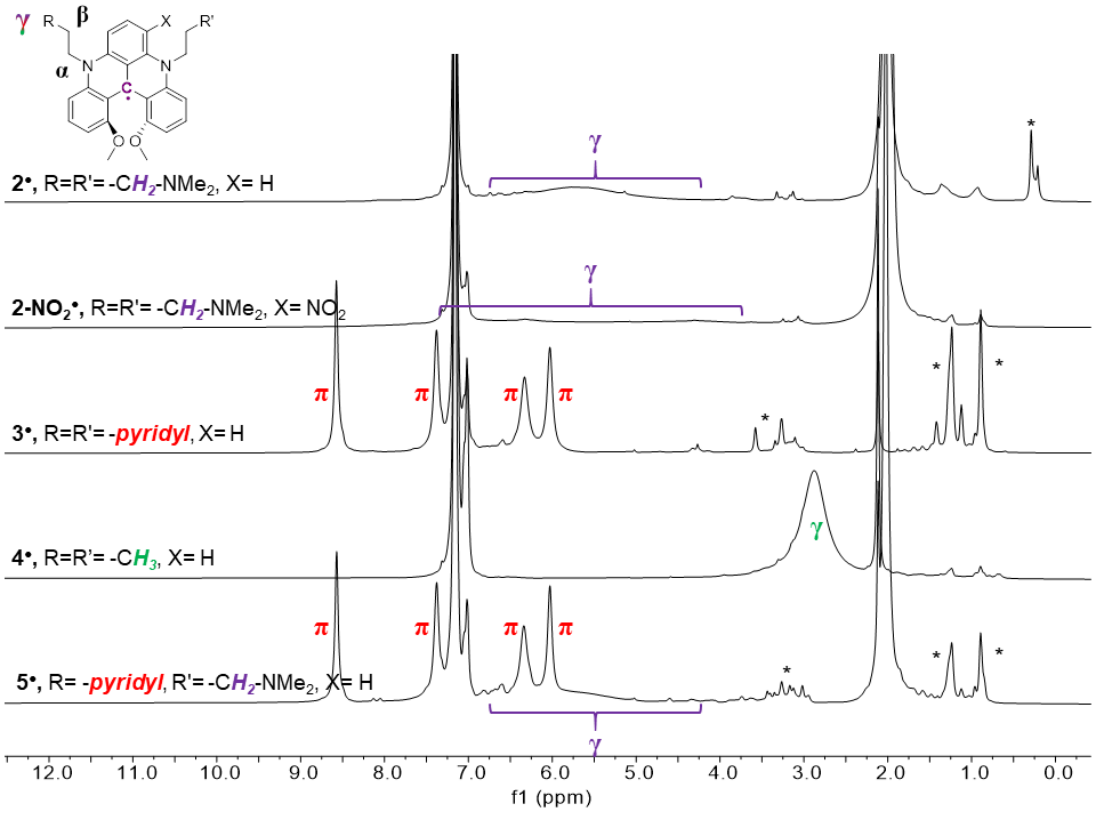

Figure S26 : ^{1}H NMR spectra of **2'-5'** in C_6D_6 at 298 K. Impurities are indicated by an asterisk (*)

IV. Single crystal X-ray Diffraction

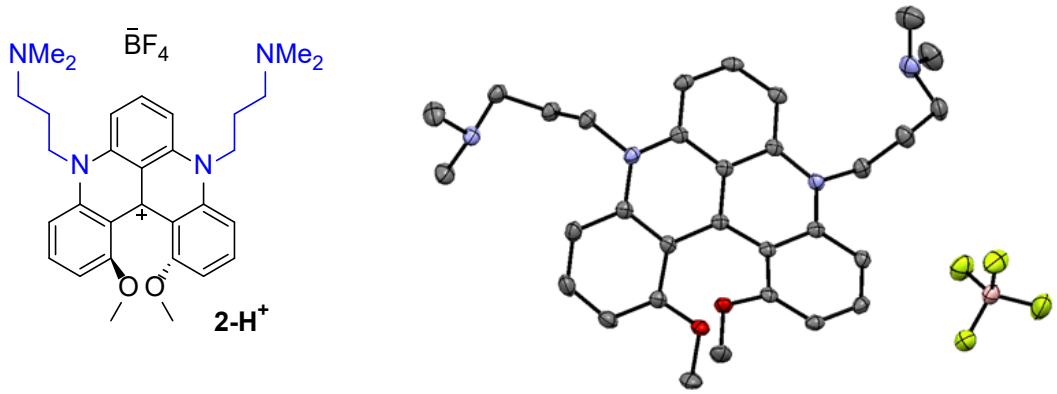

Table S1 Crystal data and structure refinement for 2-H$^+$

Identification code	2-H$^+$
CCDC	2004976
Empirical formula	$C_{32}H_{41}BCl_2F_4N_4O_2$
Formula weight	671.43
Temperature/K	100.0
Crystal system	triclinic
Space group	P-1
a/Å	11.5110(3)
b/Å	12.4254(3)
c/Å	13.1831(3)
α/°	85.1060(18)
β/°	78.778(2)
γ/°	64.945(3)
Volume/Å^3	1675.45(8)
Z	2
ρ_{calc}g/cm^3	1.3308
μ/mm^{-1}	0.251
F(000)	705.0
Crystal size/mm^3	0.3 × 0.25 × 0.2
Radiation	Mo Kα (λ = 0.71073)
2Θ range for data collection/°	6.3 to 52.74
Index ranges	-16 ≤ h ≤ 16, -17 ≤ k ≤ 17, -17 ≤ l ≤ 18
Reflections collected	35035
Independent reflections	6857 [R_{int} = 0.0227, R_{sigma} = 0.0230]
Data/restraints/parameters	6857/0/440
Goodness-of-fit on F^2	1.077
Final R indexes [I>=2σ (I)]	R_1 = 0.0460, wR_2 = 0.1040
Final R indexes [all data]	R_1 = 0.0508, wR_2 = 0.1066
Largest diff. peak/hole / e Å^{-3}	0.37/-0.25

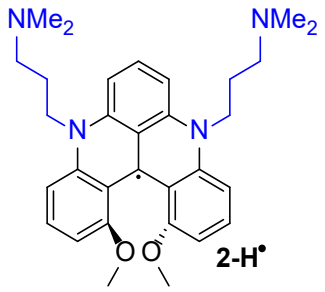

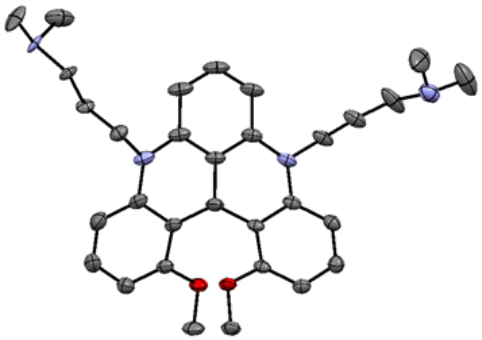

Table S2 Crystal data and structure refinement for 2-H•

Identification code	2-H•
CCDC	2004977
Empirical formula	$C_{31}H_{39}N_4O_2$
Formula weight	500.53
Temperature/K	100.0
Crystal system	orthorhombic
Space group	Pbca
a/Å	20.1829(5)
b/Å	10.7314(3)
c/Å	25.5707(7)
α/°	90
β/°	90
γ/°	90
Volume/Å^3	5538.4(3)
Z	8
ρ_{calc}g/cm^3	1.201
μ/mm^{-1}	0.382
F(000)	2155.0
Crystal size/mm^3	0.12 × 0.1 × 0.05
Radiation	GaKα (λ = 1.34138)
2Θ range for data collection/°	7.12 to 146.538
Index ranges	-27 ≤ h ≤ 24, -13 ≤ k ≤ 14, -32 ≤ l ≤ 31
Reflections collected	45766
Independent reflections	7238 [R_{int} = 0.0549, R_{sigma} = 0.0405]
Data/restraints/parameters	7238/6/414
Goodness-of-fit on F^2	1.095
Final R indexes [I>=2σ (I)]	R_1 = 0.0669, wR_2 = 0.1402
Final R indexes [all data]	R_1 = 0.0906, wR_2 = 0.1506
Largest diff. peak/hole / e Å^{-3}	0.54/-0.25

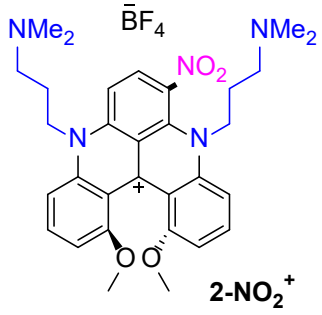

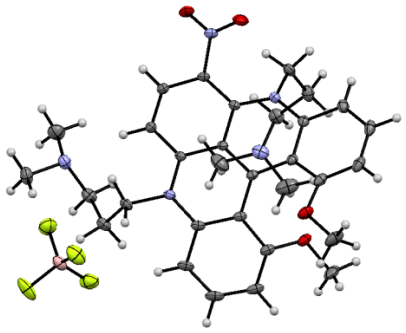

Table S3 Crystal data and structure refinement for 2-NO_2^+.

Identification code	**2-NO_2^+**
CCDC	2004974
Empirical formula	C31 H38 N5 O4
Formula weight	544.66
Temperature/K	100.0
Crystal system	triclinic
Space group	P-1
a/Å	10.834(7)
b/Å	11.010(7)
c/Å	13.357(9)
α/°	71.977(17)
β/°	84.217(17)
γ/°	64.762(17)
Volume/$Å^3$	1675.45(8)
Z	2
$\rho_{calc}g/cm^3$	1.3308
μ/mm^{-1}	0.251
F(000)	705.0
Crystal size/mm^3	0.3 × 0.25 × 0.2
Radiation	Mo Kα (λ = 0.71073)
2Θ range for data collection/°	6.3 to 52.74
Index ranges	$-16 \le h \le 16$, $-17 \le k \le 17$, $-17 \le l \le 18$
Reflections collected	35035
Independent reflections	6857 [R_{int} = 0.0227, R_{sigma} = 0.0230]
Data/restraints/parameters	6857/0/440
Goodness-of-fit on F^2	1.077
Final R indexes [I>=2σ (I)]	R_1 = 0.0460, wR_2 = 0.1040
Final R indexes [all data]	R_1 = 0.0508, wR_2 = 0.1066
Largest diff. peak/hole / e $Å^{-3}$	0.37/-0.25

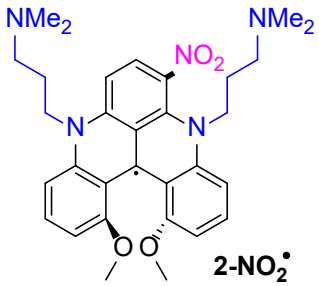

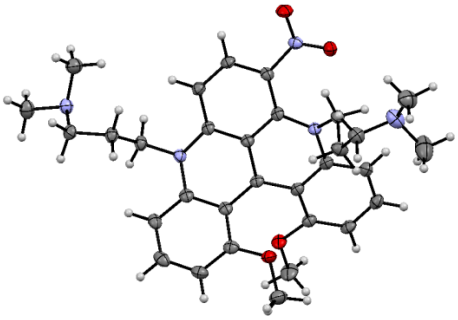

Table S4 Crystal data and structure refinement for 2-$NO_2^{\bullet}$

Identification code	**2-$NO_2^{\bullet}$**
CCDC	2004975
Empirical formula	C31 H38 N5 O4
Formula weight	544.66
Temperature/K	100.0
Crystal system	triclinic
Space group	P-1
a/Å	10.834(7)
b/Å	11.010(7)
c/Å	13.357(9)
α/°	71.977(17)
β/°	84.217(17)
γ/°	64.762(17)
Volume/$Å^3$	1369.6(16)
Z	2
$\rho_{calc}g/cm^3$	1.321
μ/mm^{-1}	0.089
F(000)	582.0
Crystal size/mm^3	0.12 × 0.1 × 0.05
Radiation	GaKα (λ = 1.34138)
2Θ range for data collection/°	7.12 to 146.538
Index ranges	-27 ≤ h ≤ 24, -13 ≤ k ≤ 14, -32 ≤ l ≤ 31
Reflections collected	45766
Independent reflections	7238 [R_{int} = 0.0549, R_{sigma} = 0.0405]
Data/restraints/parameters	7238/6/414
Goodness-of-fit on F^2	1.095
Final R indexes [I>=2σ (I)]	R_1 = 0.0669, wR_2 = 0.1402
Final R indexes [all data]	R_1 = 0.0906, wR_2 = 0.1506
Largest diff. peak/hole / e $Å^{-3}$	0.54/-0.25

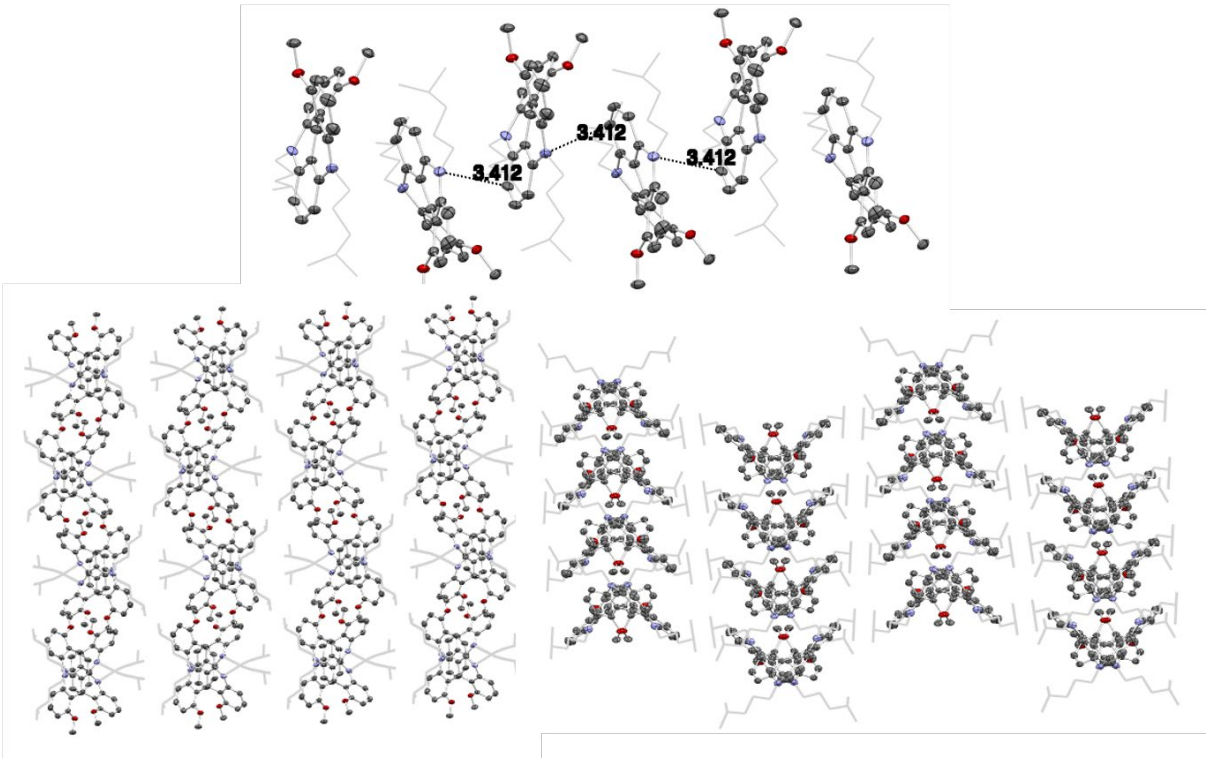

Figure S27: Packing for **2-H$^{\bullet}$** (for clarity hydrogen atoms and solvents molecules have been omitted)

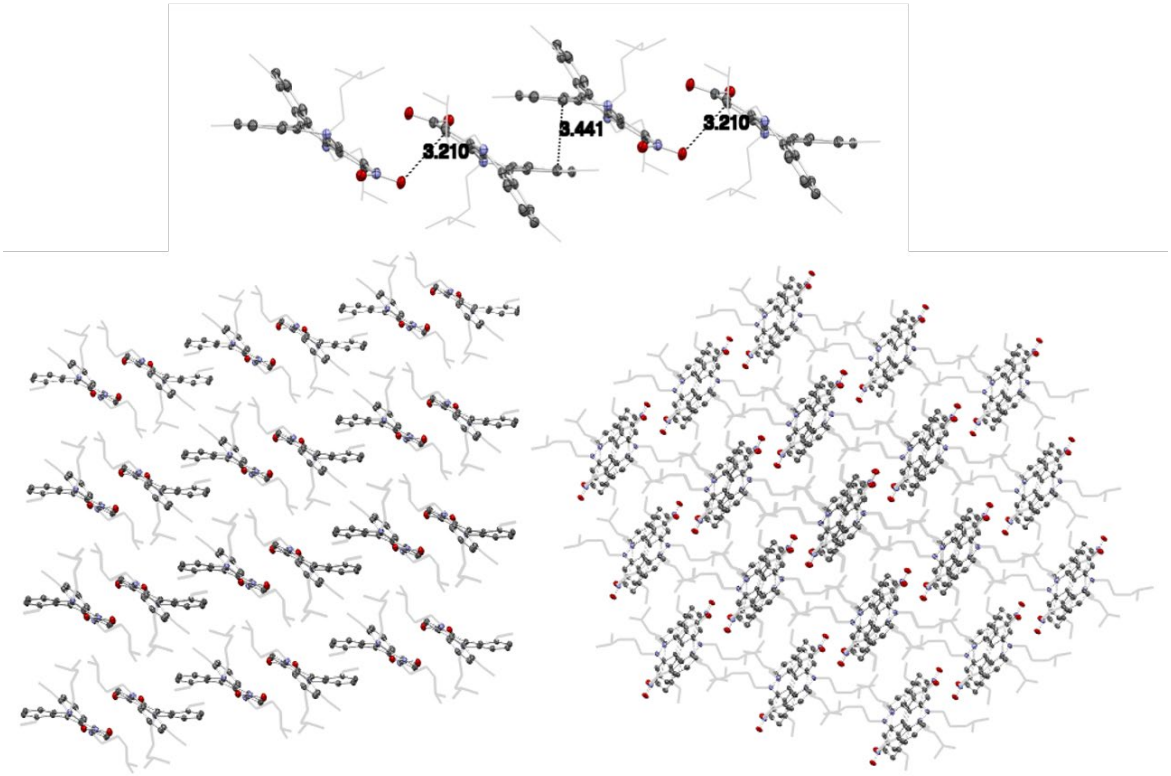

Figure S28: Packing for **2-NO$_2^{\bullet}$** (for clarity hydrogen atoms and solvents molecules have been omitted)

Table S5. Characteristic Bond lengths and bond angles for **2-H$^+$**, **2-H$^\bullet$**, **2-NO$_2^+$** and **2-NO$_2^\bullet$**

	Bonds length (Å)			
Selected Bonds and distances	**2-H$^+$**	**2-H$^\bullet$**	**2-NO$_2^+$**	**2-NO$_2^\bullet$**
C1–C2	1.406(2)	1.439(2)	1.431(1)	1.423(3)
C1–C3	1.435(3)	1.444(2)	1.413(1)	1.429(3)
C1–C4	1.431(3)	1.446(2)	1.440(1)	1.438(3)
O1···O2	2.743	2.772	2.659	2.773
C2–C5	-	-	1.435(1)	1.408(3)
C–NO$_2$	-	-	1.452(1)	1.444(3)
N2-O (NO$_2$)	-	-	1.233(1)/1.235(1)	1.226(2)/1.235(2)
	Angles (°)			
***Selected** Planes Angles*	**2-H$^+$**	**2-H$^\bullet$**	**2-NO$_2^+$**	**2-NO$_2^\bullet$**
(MeO)Ph ^ (MeO)Ph	41.93	45.92	38.37	52.05

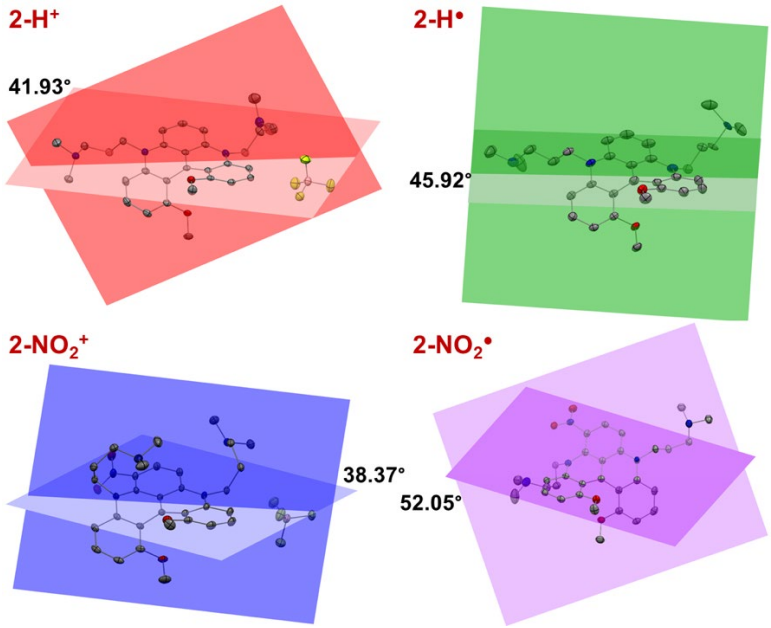

Figure S29: Distortion angle between aromatic rings MeO-Ph for **2-H$^+$**, **2-H$^\bullet$**, **2-NO$_2^+$** and **2-NO$_2^\bullet$** (for clarity hydrogen atoms and solvents molecules have been omitted).

Figure S30: Torsion angle between Me$_2$N-*n*Pr-N arm and the benzonaphthyridine core for **2-H$^\bullet$**, and **2-NO$_2^\bullet$** (for clarity hydrogen atoms and solvents molecules have been omitted)

V. EPR Spectroscopy

The continuous wave (CW) electron paramagnetic resonance (EPR) experiments were carried out at the University of Arizona EPR Facility, on the X-band EPR spectrometer Elexsys E500 (Bruker Biospin) equipped with the electron-nuclear double resonance (ENDOR) system and variable temperature nitrogen flow system.

VI. DFT Computational Details

Density functional theory (DFT) calculations[5][6] were done on a full atom scale using the unrestricted long-range corrected version[7] of the hybrid 1993 Becke three-parameter exchange functional[8]-[10] and the Lee–Yang–Parr non-local correlation functional[11] (UCAM-B3LYP) implemented in Gaussian 09, revision D.01, software.[12] The internal triple-ζ quality basis set 6-311G(d,p) was applied to all atoms. The geometry optimized models were found as minima on the potential energy surface. Molecular orbitals (MO) and self-consistent field (SCF) spin density surfaces were obtained using the cubegen utility in Gaussian 09. All calculations were executed on the Ocelote cluster at the University of Arizona High Performance Computing center.

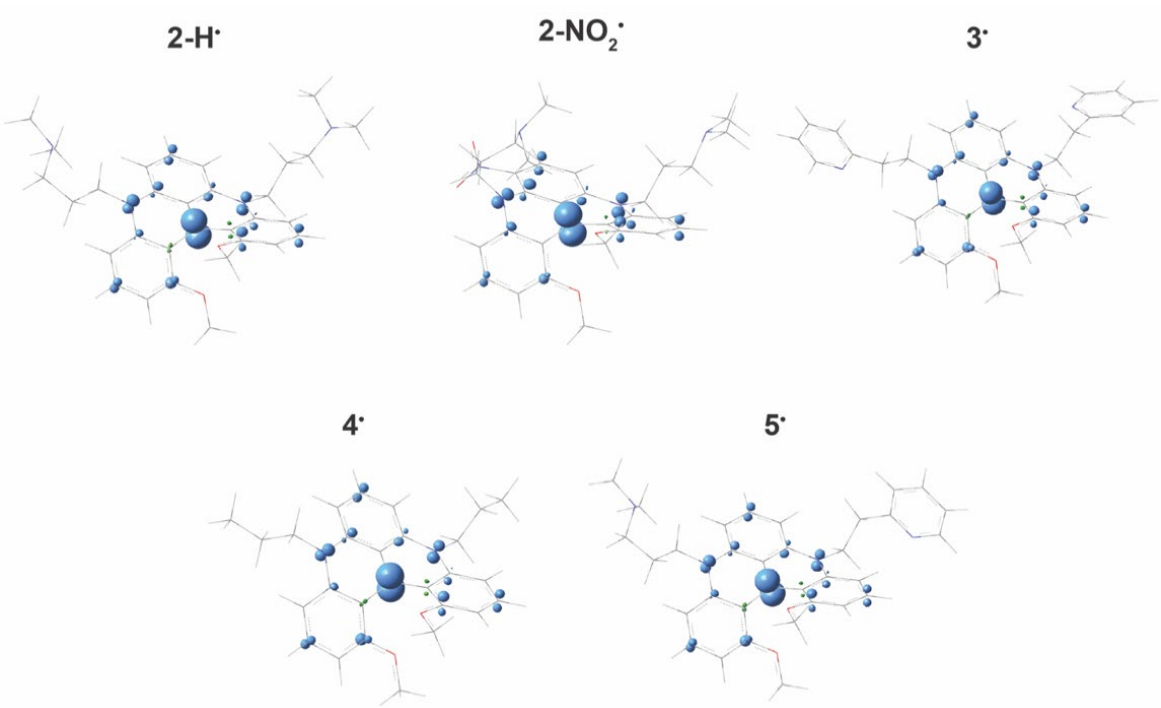

Figure S31. Spin density distribution for the calculated open-shell doublet models of **2–5**˙. Surfaces were plotted at a 0.015 isovalue.

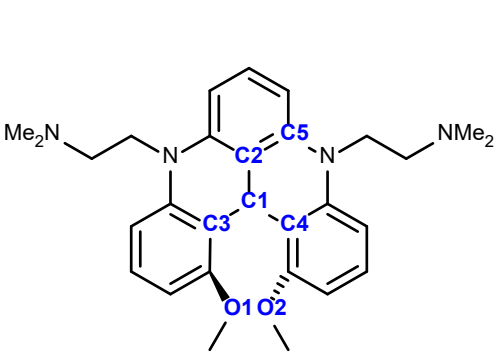

2-H

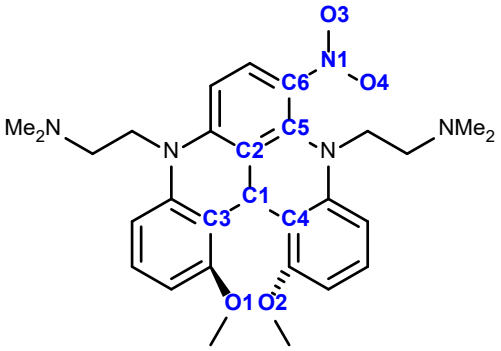

2-NO$_2$

Table S6. Selected bond distances from the X-ray single crystal structures and DFT geometry optimized structures for **2-H**$^{\bullet}$ and **2-NO$_2$**$^{\bullet}$.

Atom	**2-H**$^{\bullet}$		**2-NO$_2$**$^{\bullet}$	
Labels	**Exp.**	**DFT**	**Exp.**	**DFT**
C1-C2	1.439(2)	1.430	1.423(3)	1.429
C1-C3	1.444(2)	1.443	1.429(3)	1.440
C1-C4	1.446(2)	1.442	1.438(3)	1.446
O1---O2	2.772	2.744	2.773	2.760
C2-C5	-		1.408(3)	1.412
C6-N1	-		1.444(3)	1.458
N1-O3	-		1.226(2)	1.219
N1-O4	-		1.235(2)	1.218

Table S7. Selected angles from the X-ray single crystal structures and DFT geometry optimized structures for **2-H**$^{\bullet}$ and **2-NO$_2$**$^{\bullet}$.

Atom	**2-H**$^{\bullet}$		**2-NO$_2$**$^{\bullet}$	
Labels	**Exp.**	**DFT**	**Exp.**	**DFT**
O1-C1-O2	58.85	58.57	59.64	58.78

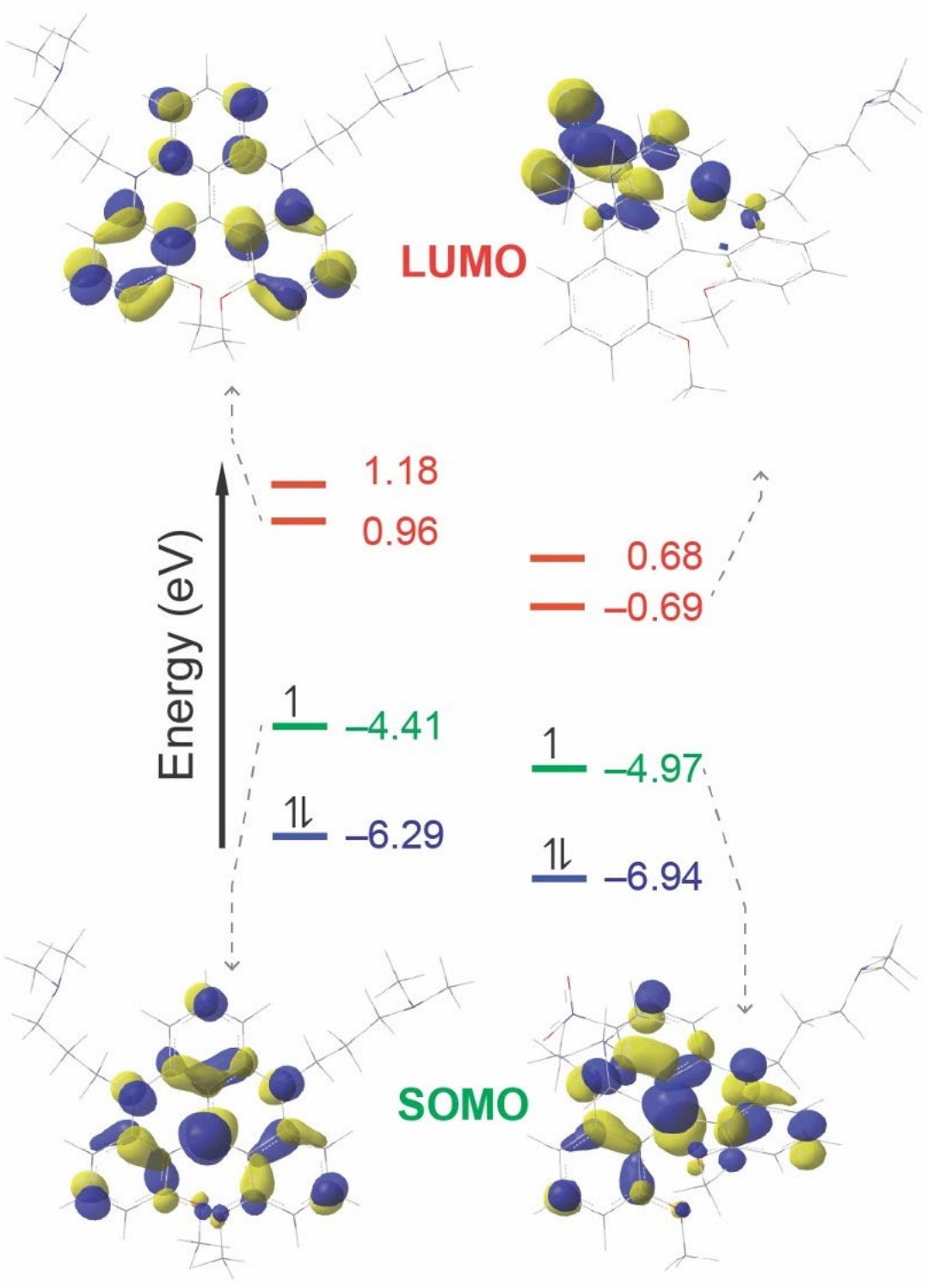

Figure S32. Frontier molecular orbital diagram of **2-H**$^{\bullet}$ (left) and **2-NO$_2$**$^{\bullet}$ (right) Percentage orbital contribution across the central carbon is also shown. Surfaces were plotted at a 0.04 isovalue.

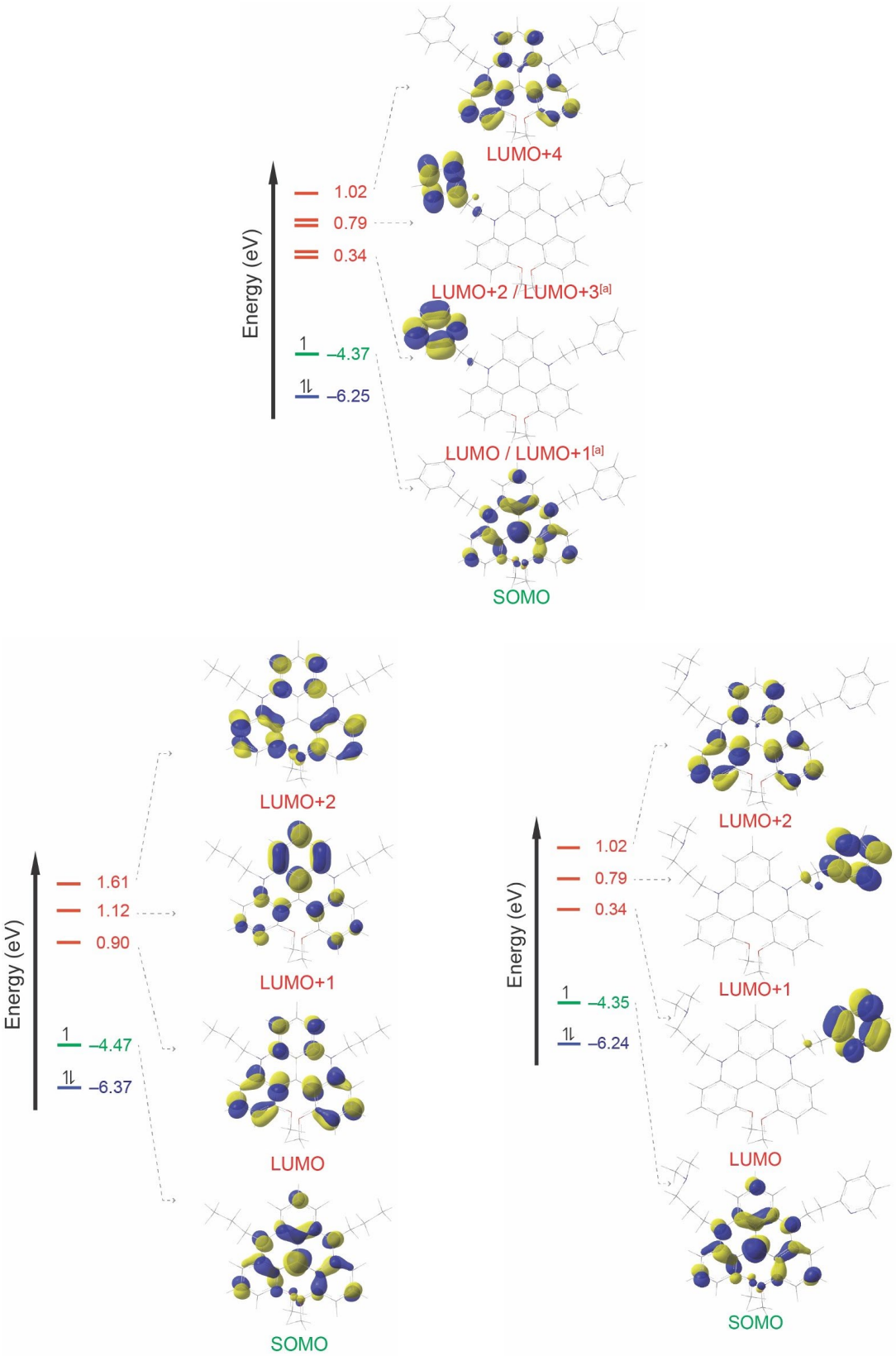

Figure S33. Frontier MO diagram for the calculated DFT model of **3**˙ (top), **4**˙(bottom left), and **5**˙(bottom, right). Iso-surfaces corresponding to the alpha orbitals of the model are shown at a 0.04 value. The set of degenerate MOs in **3**˙ corresponds to the same π^* interaction located in the opposite pyridine moiety.

VII. UV-vis Spectra Analysis

VII.1 UV-vis Spectroscopy under anaerobic conditions

Absorption spectra were recorded on a ThermoScientific Evolution 220 UV-Visible spectrophotometer at 25 ˚C in analytical-grade solvents (con. 10-5 M). All UV samples for spectroscopy were prepared under an inert atmosphere in a Mbraun Labmaster glovebox maintained at less than 1 ppm O_2. A 3 mL gas-tight cuvette (Quartz Cuvette Self Masking Screw Cap) was used for anaerobic acquisition of spectra. All radicals decay kinetics were studied in the presence of oxygen, solutions of **2˙–5˙** in CF_3-toluene prepared in a N_2-filled glove box were exposed to air and monitored by UV−vis spectroscopy over time.

The compounds **2-H**$^+$, **3**$^+$-**5**$^+$ show similar spectrum with three distinct absorption in the visible regions (λ > 350nm), indicating that the nitrogen bridge substituents have a negligible effect on the transition energy (Figure S29, and Table S6). A sharp peak around 620 nm (ε > 14000), a shoulder at 570 nm (ε > 10000), and a broad absorption around 430 nm (ε > 6000). All four radicals, **2-H˙**, **3˙-5˙** have a sharp absorption band with the maximum absorbance around 390 nm (ε > 15000), a shoulder at around 450 nm (ε > 5000), and a broad absorption peak around 560 nm (ε > 6000) (Figure S40, and Table S6).

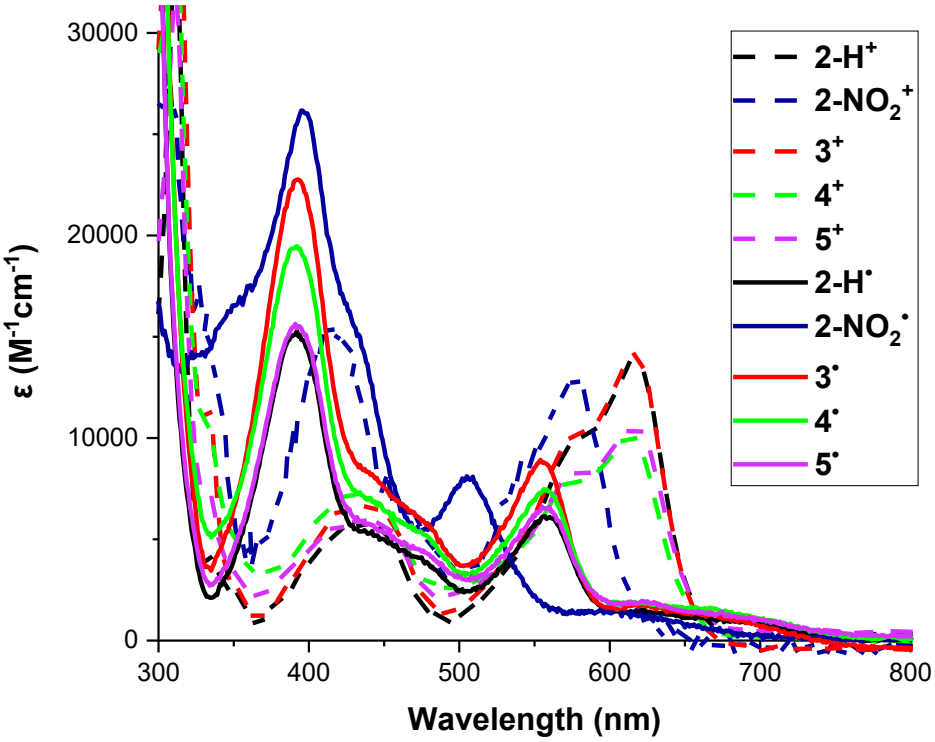

Figure S34. Combined UV-visible absorption spectra for **2**$^+$-**5**$^+$ (dashed line) and **2˙-5˙** (solid line).

Table S8. Main features of UV-vis spectra of compounds of compounds **2-5** in *α,α,α*-Trifluorotoluene

Compound	λ_{max} absorption [nm] (ε [$M^{-1}.cm^{-1}$])
2-H$^+$	435 (6044), 577 (10526), 617 (14431)
2-H$^\bullet$	392 (15936), 445 (5093), 558 (6496)
2-NO$_2^+$	417 (18320), 576 (12854)
2-NO$_2^\bullet$	395 (26172), 505 (8116), 604 (1559)
3$^+$	433 (7501), 574 (10987), 612 (14925)
3$^\bullet$	392 (23422), 444 (8061), 554 (9555)
4$^+$	434 (7325), 570 (7706), 613 (10006)
4$^\bullet$	392 (19476), 476 (5245), 556 (7469)
5$^+$	440 (6368), 572 (8705), 615 (11032)
5$^\bullet$	391 (16222), 473 (5229), 557 (7160)

VII.2 Monitoring of radical decay upon exposure to air by UV-vis Spectroscopy.

To quantify the stability of all radicals in the presence of oxygen, solutions of **2$^\bullet$**–**5$^\bullet$** in CF_3-toluene prepared in a N_2-filled glove box were exposed to air and monitored by UV−vis spectroscopy over time. The absorption spectrum of the cation and their radical analog under N2 atmosphere are shown in Figure S36, S38, S40, S42 and S44. The change in absorption spectroscopy for radical **2-H$^\bullet$**, **2-NO$_2^\bullet$**, and **3$^\bullet$-5$^\bullet$** after exposure to air are shown in Figure S37, S39, S41, S43 and S45 respectively, and show a slow decreased with time, reaching the lowest absorption limit within hours.

The first order decay of the absorption of each radical as well as their $t_{1/2}$ is shown in Figure S35.

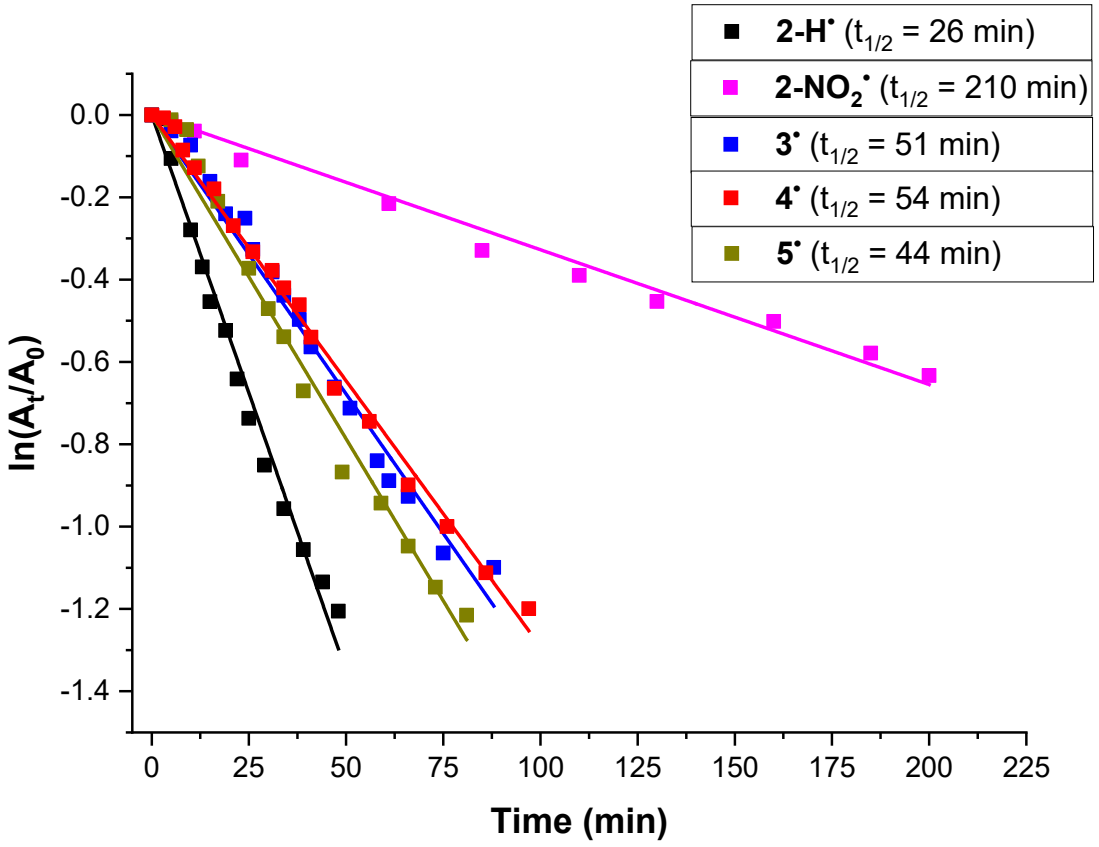

Figure S35. Plot of the first order decay of the absorbance for radical **2•-5•**

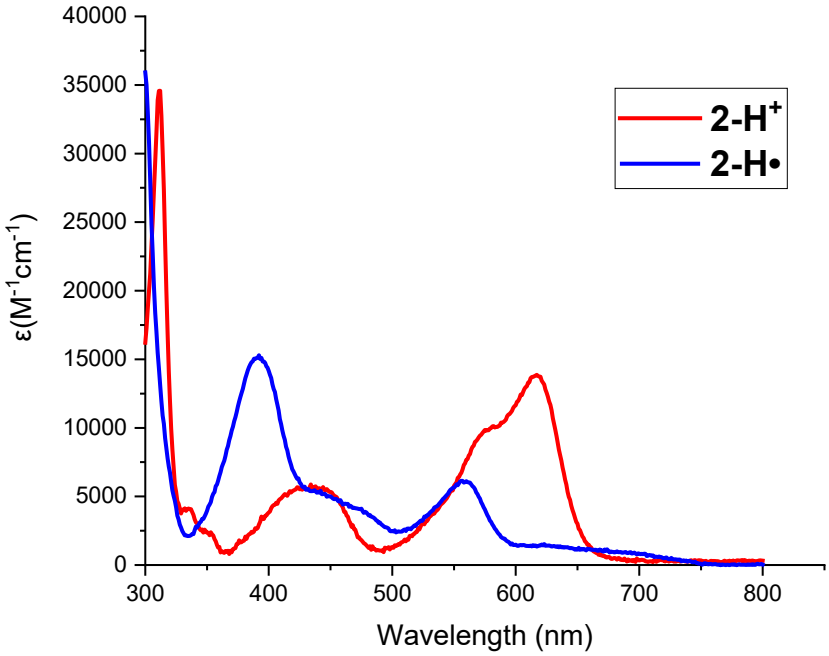

Figure S36: UV−vis spectra (6.8×10^{-5} M in CF_3-Toluene, room temperature) of **2-H$^+$**

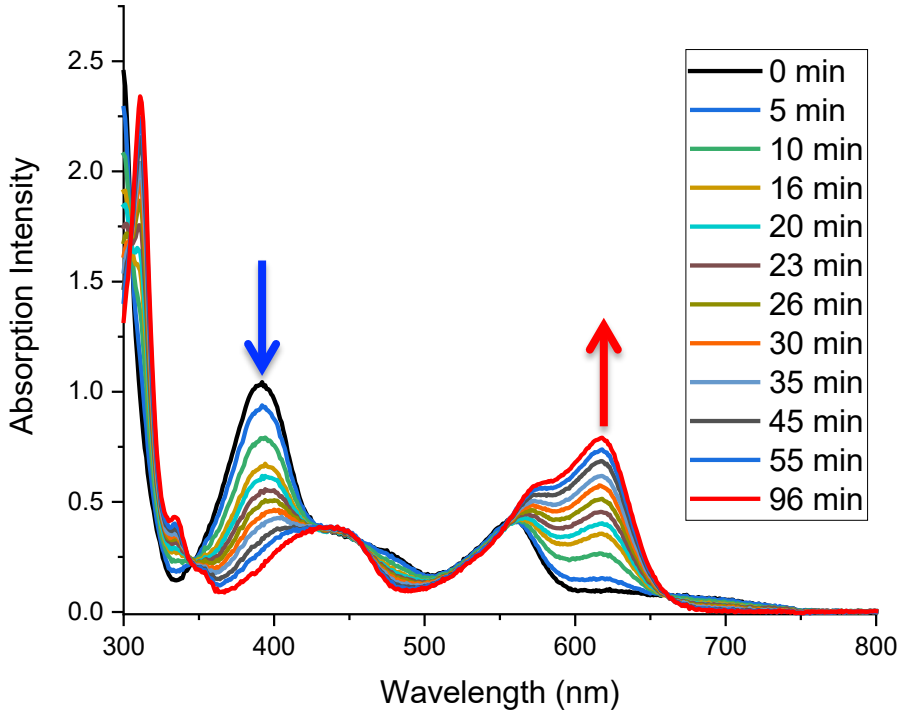

Figure S37. Change of UV-visible absorption spectra for **2-H$^{\bullet}$** (6.8×10^{-5} M) with time after exposure to air

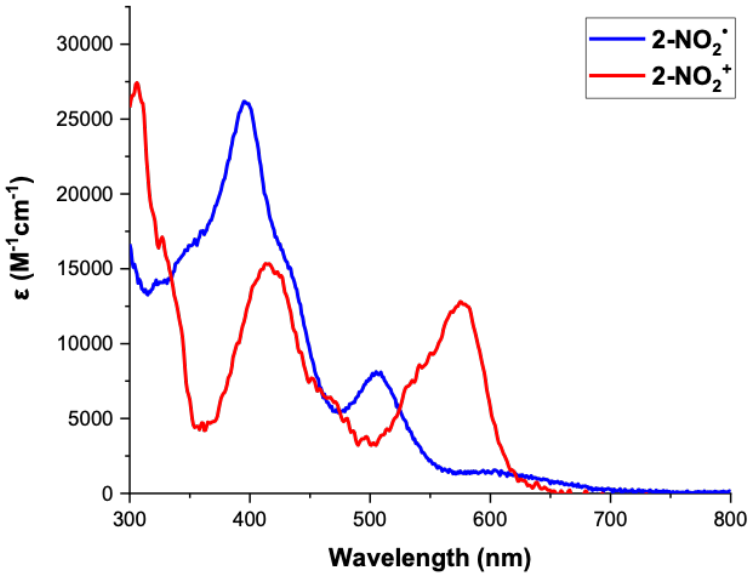

Figure S38: UV−vis spectra (5.9×10^{-5} M in CF_3-Toluene, room temperature) of **2-NO_2**

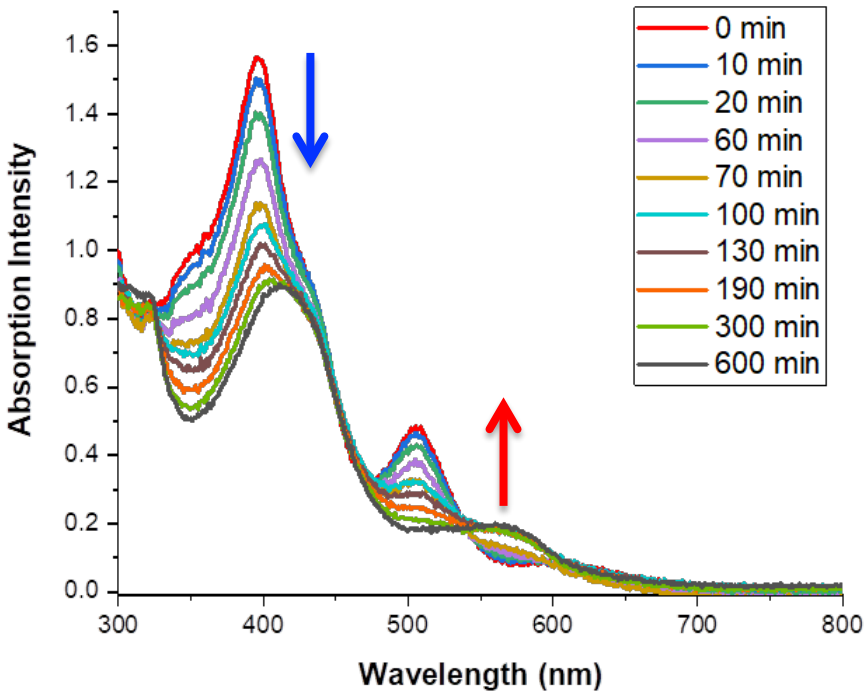

Figure S39. Change of UV-visible absorption spectra for **2-$NO_2^{\bullet}$** (5.9×10^{-5} M) with time after exposure to air

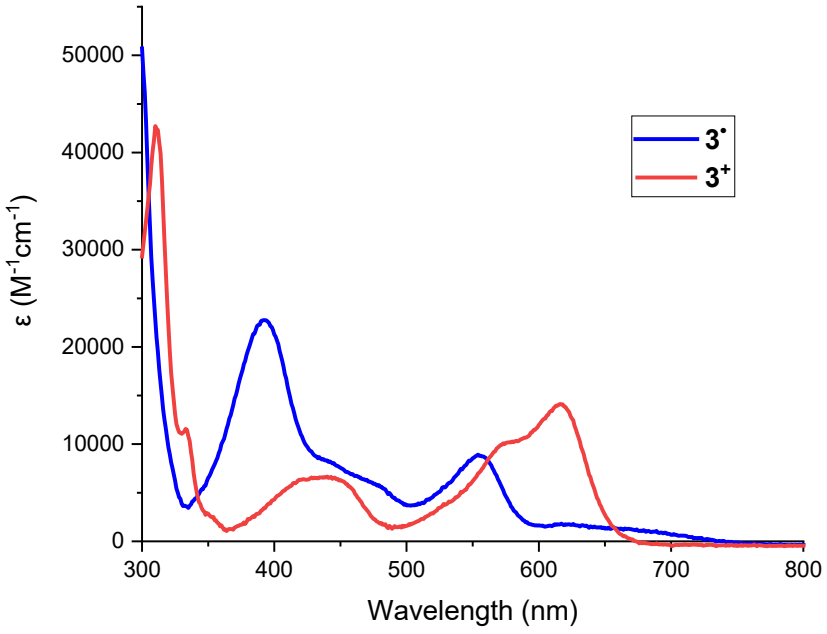

Figure S40: UV−vis spectra (6.5×10^{-5} M in CF_3-Toluene, room temperature) of **3**

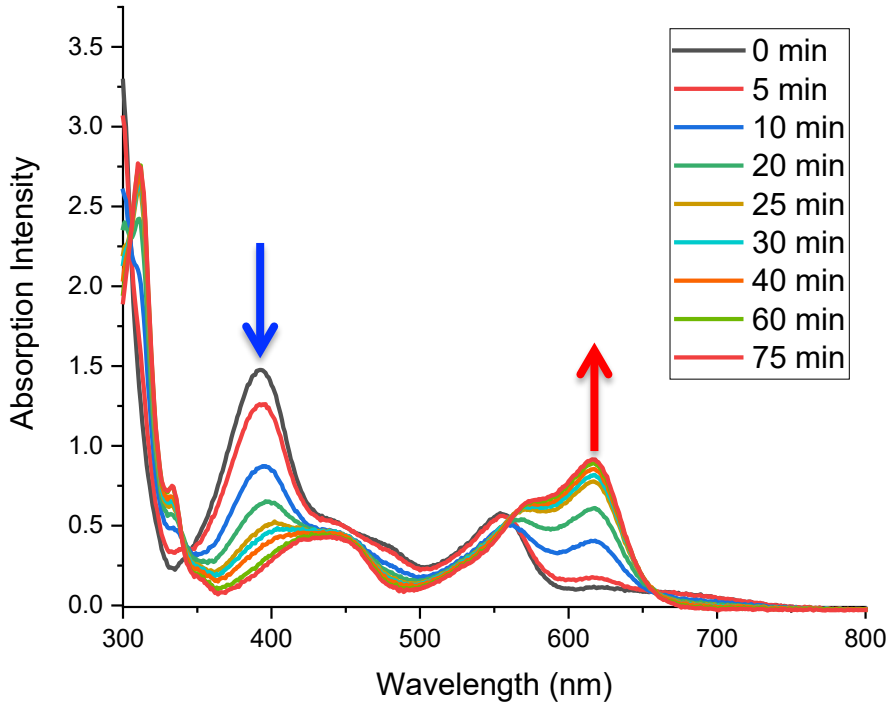

Figure S41. Change of UV-visible absorption spectra for **3•** (6.5 x 10^{-5} M) with time after exposure to air

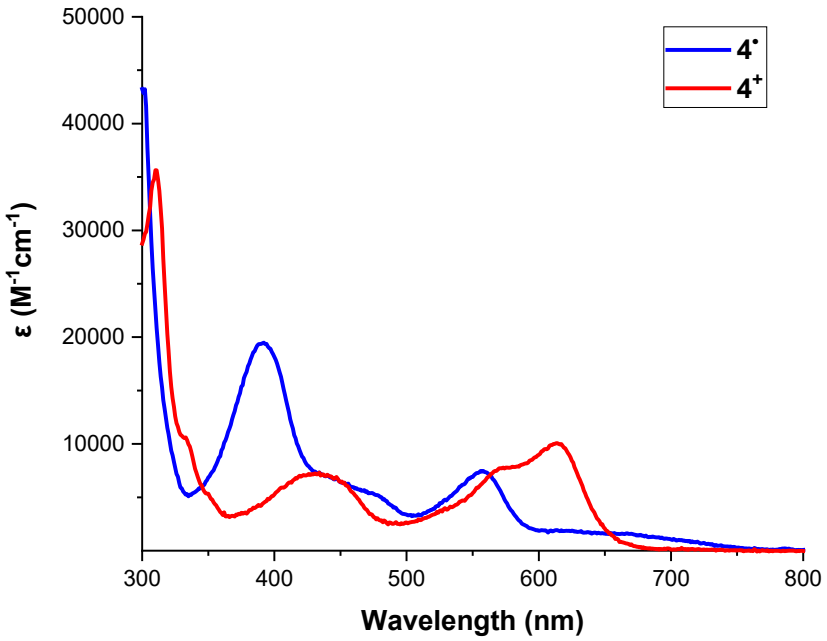

Figure S42: UV−vis spectra (8.7 × 10−5 M in CF_3-Toluene, room temperature) of **4**

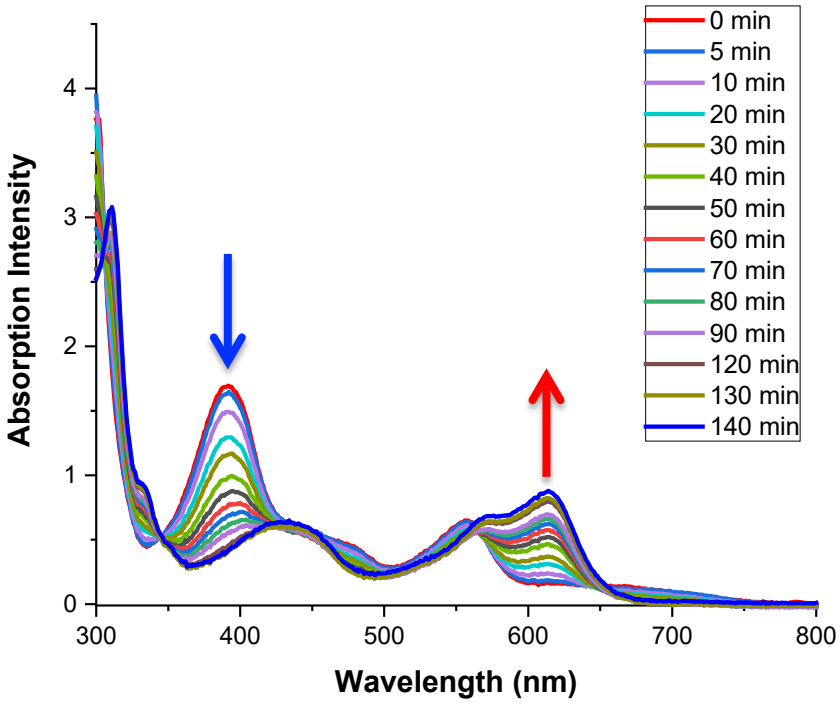

Figure S43. Change of UV-visible absorption spectra for **4•** (8.7 × 10−5 M) with time after exposure to air

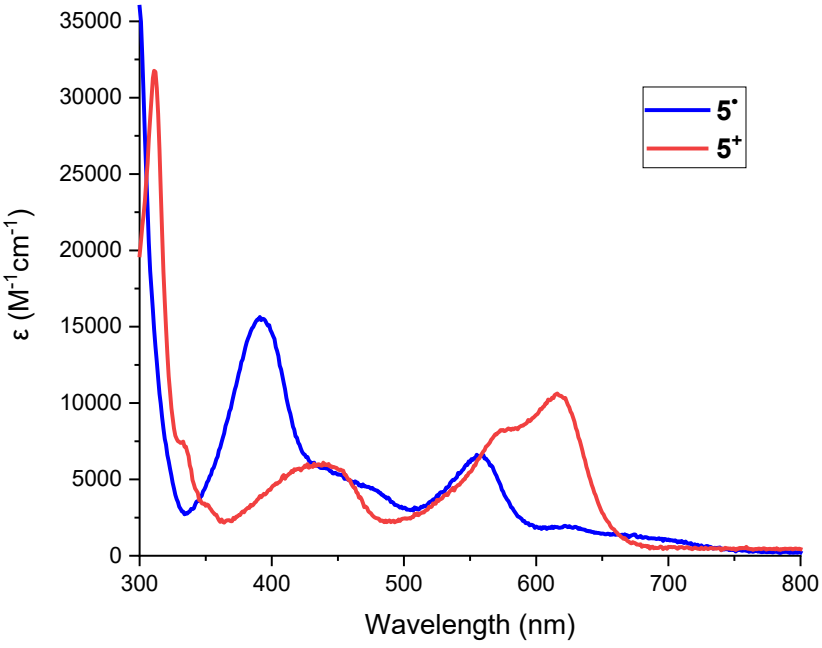

Figure S44: UV−vis spectra (6.3× 10^{-5} M in CF_3-Toluene, room temperature) of **5**

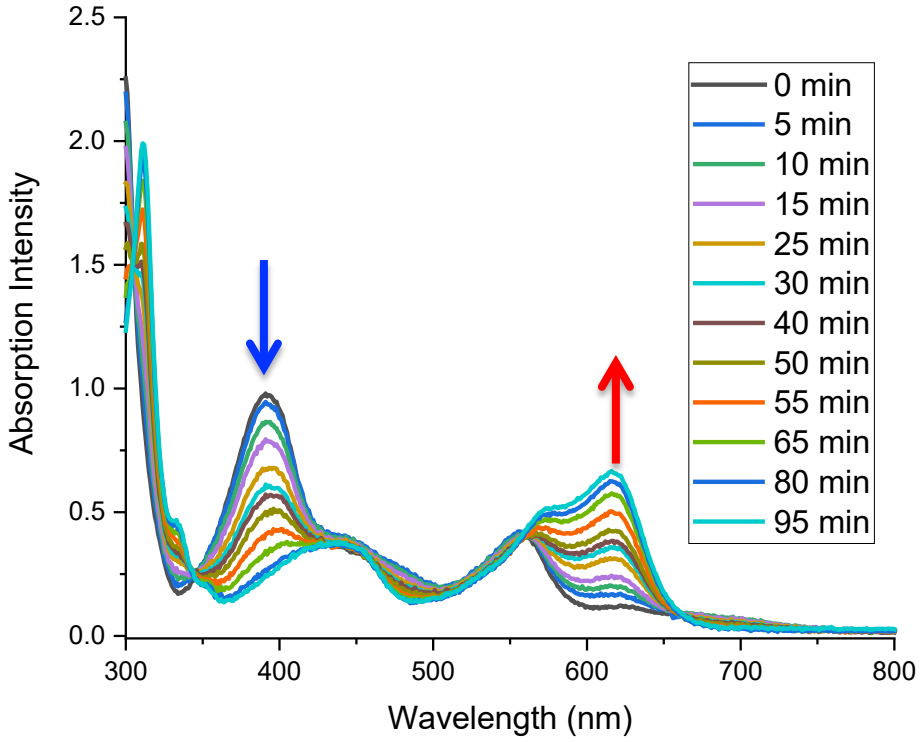

Figure S45. Change of UV-visible absorption spectra for **5˙** (6.3×10^{-5} M) with time after exposure to air

VIII. Cyclic Voltammetry

Note: Cyclic voltammograms of $\mathbf{2}^{+}$-$\mathbf{5}^{+}$ (2 mM) in DCM ([TBA][PF_6] 0.1 M) solutions recorded at a platinum working electrode (n = 0.1 V/s) and Ag/Ag^{+} as internal reference electrode, Fc/Fc^{+} was used as secondary reference by setting its $E_{1/2} = 0$. The arrows indicate the direction of the scan. All the cyclic voltammograms were recorded at ambient temperature.

VIII.1 CV data for $\mathbf{2\text{-}H}^{+}$

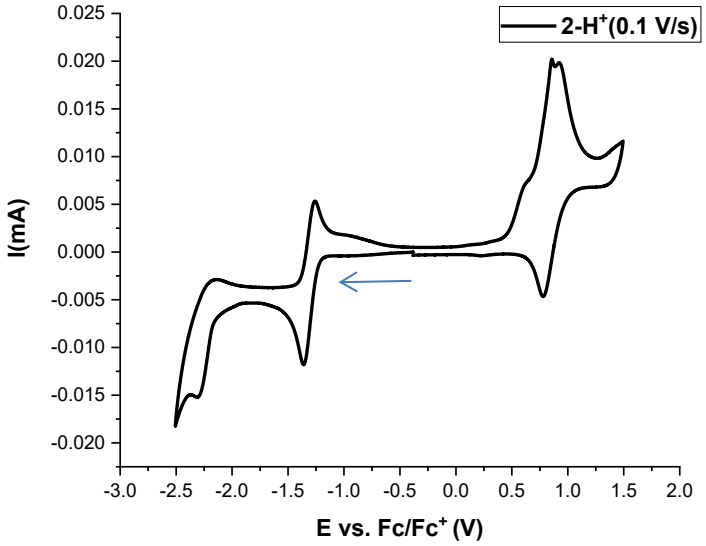

Figure S46. A cyclic voltammogram of $\mathbf{2\text{-}H}^{+}$ (2 mM) in CH_2Cl_2 ([TBA][PF_6] 0.1 M) solutions

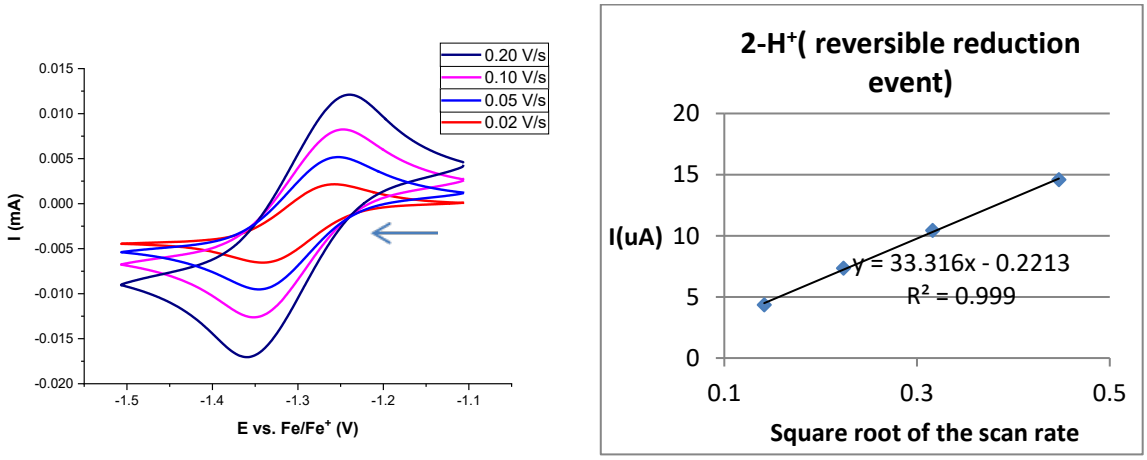

Figure S47. A reversible reduction cyclic voltammogram of $\mathbf{2\text{-}H}^{+}$ (2 mM) in CH_2Cl_2 ([TBA][PF_6] 0.1 M) solutions

VII.2 CV data for 2-NO_2^+

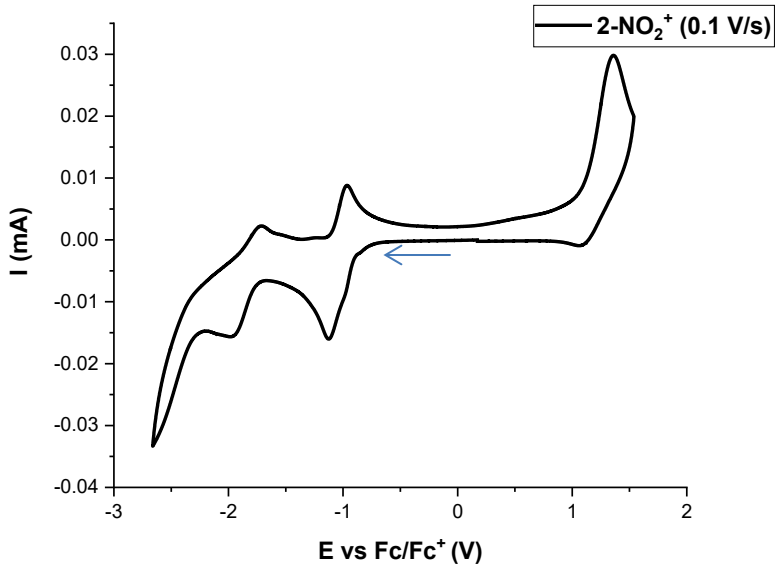

Figure S48. A cyclic voltammogram of **2-NO_2^+** (2 mM) in CH_2Cl_2 ([TBA][PF_6] 0.1 M) solutions

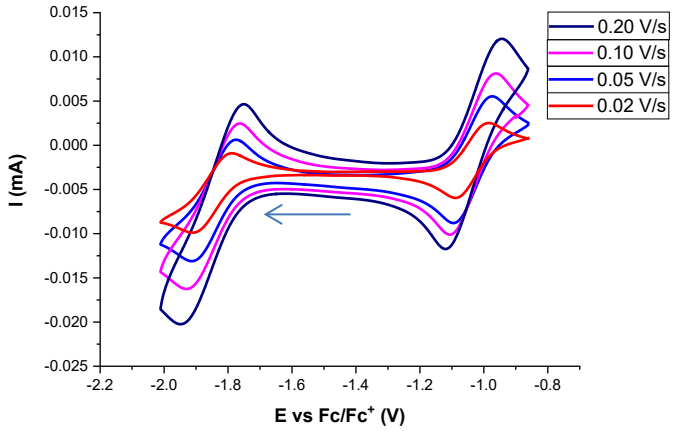

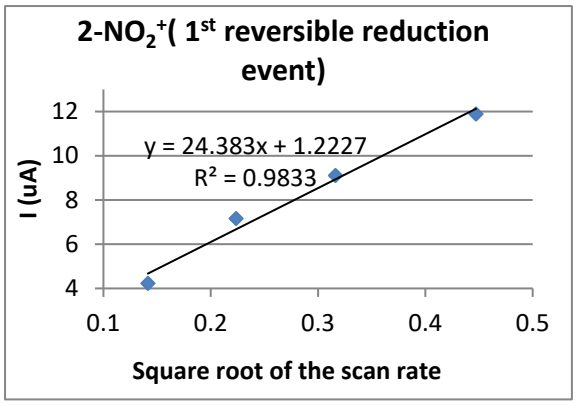

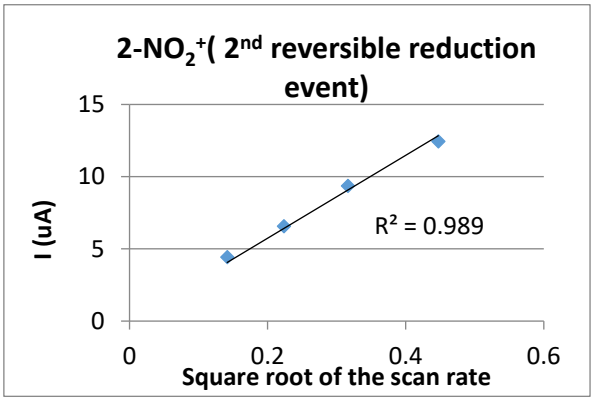

Figure S49. A reversible reduction cyclic voltammogram of **2-NO_2^+** (2 mM) in CH_2Cl_2 ([TBA][PF_6] 0.1 M) solutions

VII.3 CV data for 3^+

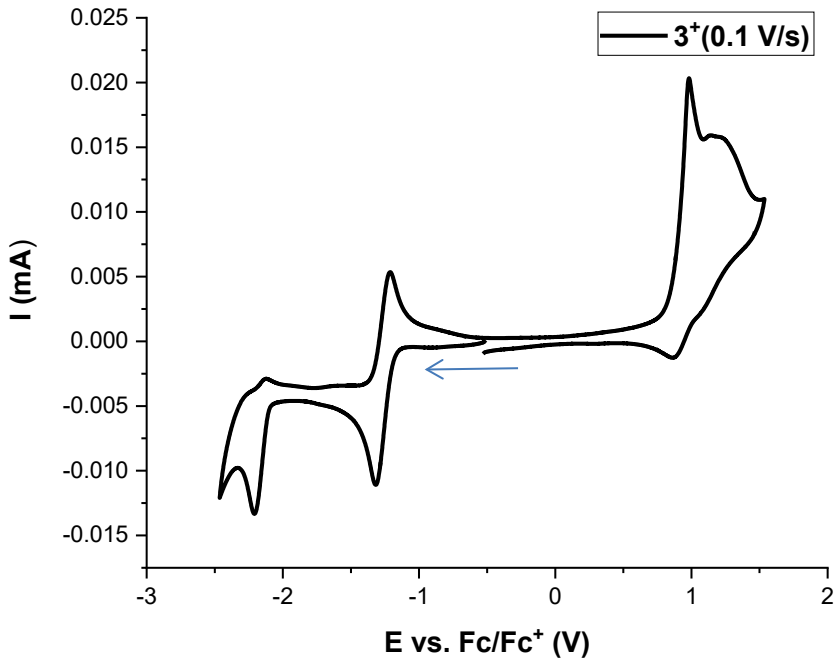

Figure S50. A cyclic voltammogram of $\mathbf{3}^+$ (2 mM) in CH_2Cl_2 ([TBA][PF_6] 0.1 M) solutions

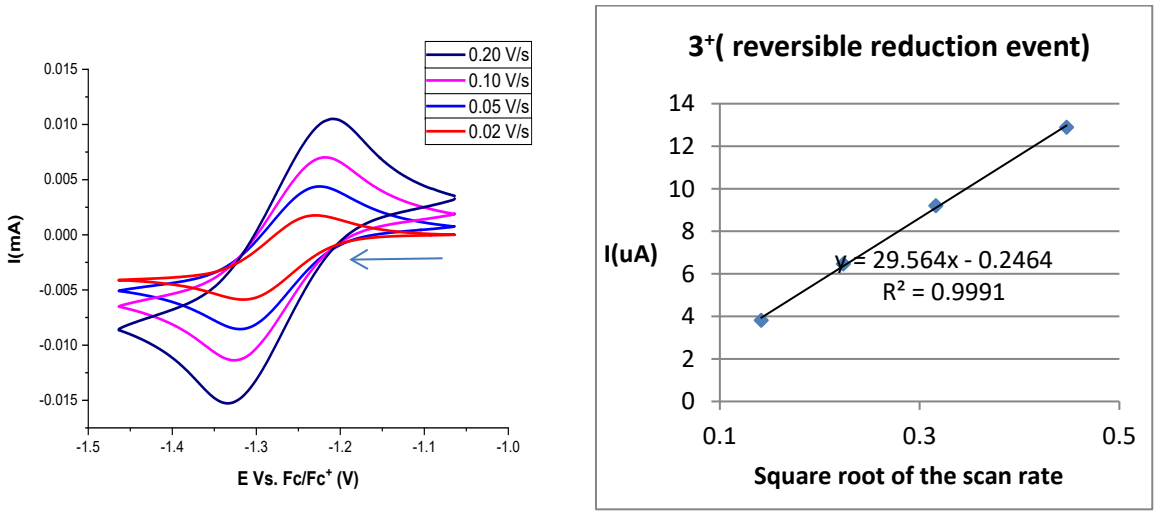

Figure S51. A reversible reduction cyclic voltammogram of $\mathbf{3}^+$ (2 mM) in CH_2Cl_2 ([TBA][PF_6] 0.1 M) solutions

VIII.4 CV data for 4^+

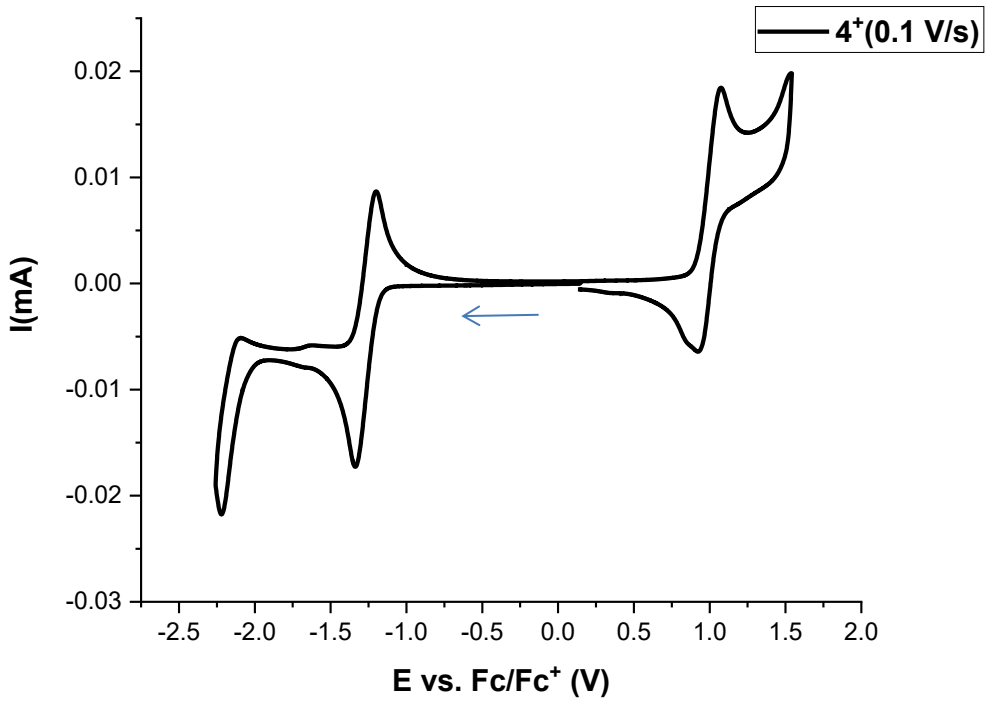

Figure S52. A cyclic voltammogram of $\mathbf{4}^+$ (2 mM) in CH_2Cl_2 ([TBA][PF_6] 0.1 M) solutions

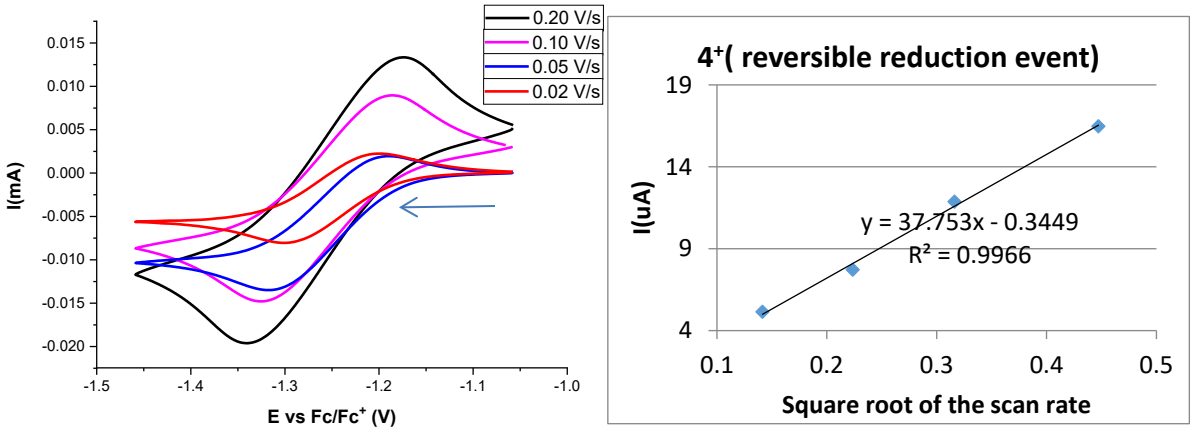

Figure S53. A first reversible reduction cyclic voltammogram of $\mathbf{4}^+$ (2 mM) in CH_2Cl_2 ([TBA][PF_6] 0.1 M) solutions

VIII.5 CV data for 5^+

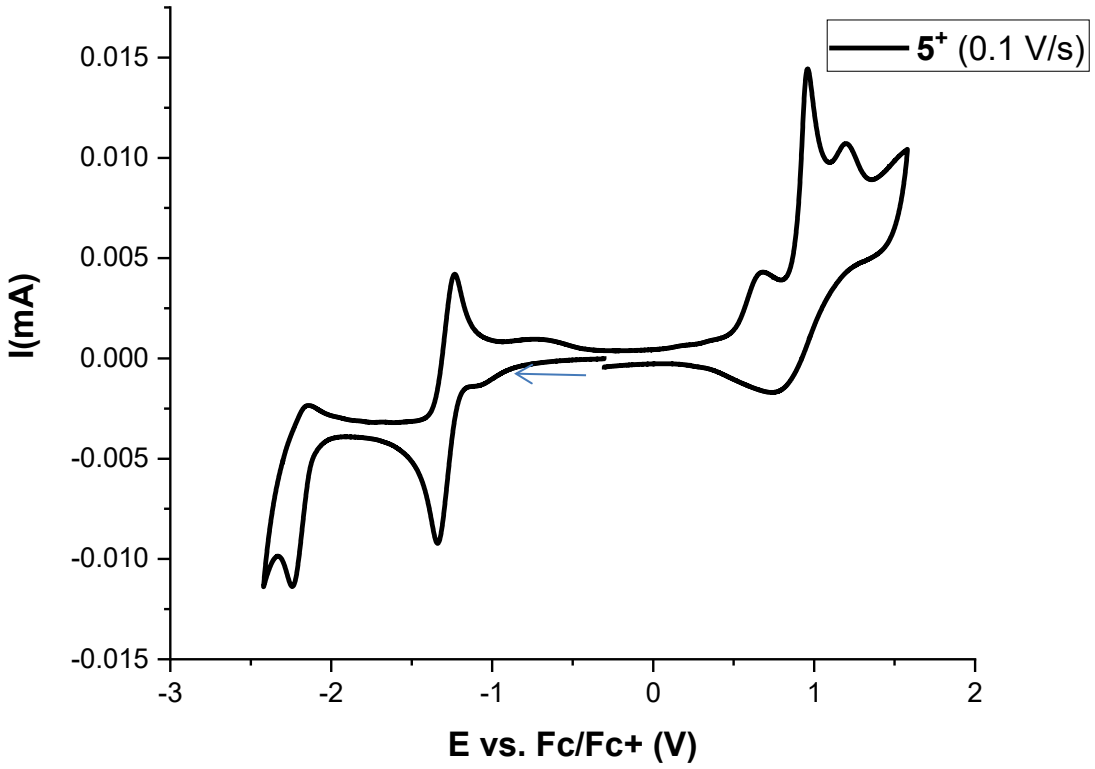

Figure S54. A cyclic voltammogram of $\mathbf{5}^+$ (2 mM) in CH_2Cl_2 ([TBA][PF_6] 0.1 M) solutions

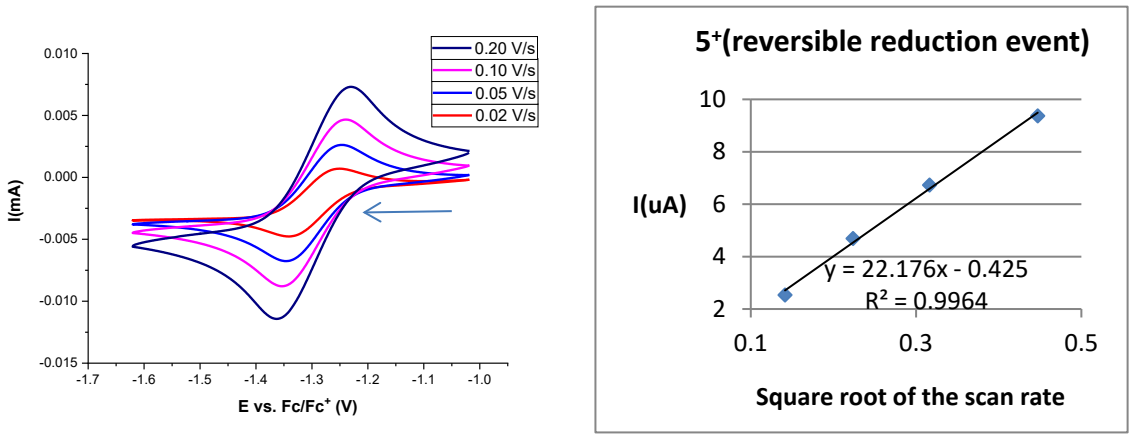

Figure S55. A second reversible reduction cyclic voltammogram of $\mathbf{5}^+$ (2 mM) in CH_2Cl_2 ([TBA][PF_6] 0.1 M) solutions

References

(1) a) B. W. Laursen, F. C. Krebs, M. F. Nielsen, K. Bechgaard, J. B. Christensen, and N. Harrit *J. Am. Chem. Soc*. 1998, **120**, 12255-12263; b) L. Mei, J. M. Veleta, and T. L. Gianetti, *J. Am. Chem. Soc*. 2020, **142**, 28, 12056–12061

(2) L. Mei, J. M. Veleta, J. Bloch, H. J. Goodman, D. Pierce-Navarro, A. Villalobos, T. L. Gianetti, *Dalton Trans.* 2020, doi.org/ 10.1039/D0DT00419G.

(3) Urben, P. G. *Bretherick's Handbook of Reactive Chemical Hazards, 7th ed,*; Academic Press Burlington, MA, 2007

(4) ESPI Metals. Potassium MSDS No. 7440-09-7; Ashland, OR, July 2015, https://www.espimetals.com/index.php/msds/232-Potassium

(5) Patterson, J. D. *Density-Functional Theory of Atoms and Molecules*; Oxford University Press: Oxford, 1989.

(6) Hohenberg, P.; Kohn, W. "Inhomogeneous Electron Gas". *Phys. Rev.* 1964, **136**, B864–B871. [DOI:10.1103/PhysRev.136.B864].

(7) Yanai, T.; Tew, D. P.; Handy, N. C. "A New Hybrid Exchange–Correlation Functional Using the Coulomb-Attenuating Method (CAM-B3LYP)". *Chem. Phys. Lett.* 2004, **393**, 51–57.

(8) Becke, A. D. "A New Mixing of Hartree–Fock and Local Density-functional Theories". *J. Chem. Phys.* 1993, **98**, 1372–1377. [DOI:10.1063/1.464304].

(9) Becke, A. D. "Density-functional Thermochemistry. III. The Role of Exact Exchange". *J. Chem. Phys.* 1993, **98**, 5648–5652. [DOI:10.1063/1.464913].

(10) Becke, A. D. "Density-Functional Exchange-Energy Approximation with Correct Asymptotic Behavior". *Phys. Rev. A* 1988, **38**, 3098–3100. [DOI:10.1103/PhysRevA.38.3098].

(11) Lee, C.; Yang, W.; Parr, R. G. "Development of the Colle-Salvetti Correlation-Energy Formula into a Functional of the Electron Density". *Phys. Rev. B* 1988, **37**, 785–789. [DOI:10.1103/PhysRevB.37.785].

(12) Frisch, M. J.; Trucks, G. W.; Schlegel, H. B.; Scuseria, G. E.; Robb, M. A.; Cheeseman, J. R.; Scalmani, G.; Barone, V.; Mennucci, B.; Petersson, G. A.; et al. "Gaussian 09". Gaussian Inc.: Wallingford, CT 2016.